

Numerical study of the $\mathcal{N} = 2$ Landau–Ginzburg model

Okuto Morikawa¹ and Hiroshi Suzuki^{1,*}

¹*Department of Physics, Kyushu University 744 Motoooka, Nishi-ku, Fukuoka, 819-0395, Japan*

**E-mail: hsuzuki@phys.kyushu-u.ac.jp*

21/8/2018

.....
 It is believed that the two-dimensional massless $\mathcal{N} = 2$ Wess–Zumino model becomes the $\mathcal{N} = 2$ superconformal field theory (SCFT) in the infrared (IR) limit. We examine this theoretical conjecture of the Landau–Ginzburg (LG) description of the $\mathcal{N} = 2$ SCFT by numerical simulations on the basis of a supersymmetric-invariant momentum-cutoff regularization. We study a single supermultiplet with cubic and quartic superpotentials. From two-point correlation functions in the IR region, we measure the scaling dimension and the central charge, which are consistent with the conjectured LG description of the A_2 and A_3 minimal models, respectively. Our result supports the theoretical conjecture and, at the same time, indicates a possible computational method of correlation functions in the $\mathcal{N} = 2$ SCFT from the LG description.

Subject Index B16, B24, B34

arXiv:1805.10735v2 [hep-lat] 18 Aug 2018

	Contents	PAGE
1	Introduction	2
2	Formulation	4
2.1	The classical action	4
2.2	Momentum cutoff regularization	5
2.3	Nicolai map	6
3	Simulation setup and classification of configurations	8
4	SUSY Ward–Takahashi relation	10
5	Scaling dimension	15
6	Central charge	19
6.1	Central charge from the supercurrent correlator	20
6.2	Central charge from the energy–momentum tensor correlator	23
6.3	Central charge from the $U(1)$ current correlator	26
7	Conclusion	26
A	Symmetries and the Noether currents	27
A.1	SUSY and the supercurrent	27
A.2	Translational invariance and the energy–momentum tensor	29
A.3	$U(1)$ symmetry and the $U(1)$ current	30
A.4	Massless free WZ model	31
B	A fast algorithm for the Jacobian computation	32

1. Introduction

In sufficiently low energies, any quantum field theory is expected to become scale invariant, all massive modes being decoupled. Such a scale-invariant theory would be described by a conformal field theory (CFT). If this low-energy theory gives rise to a nontrivial CFT, the original field theory is called the Landau–Ginzburg (LG) model or the LG description of the CFT [1]. The LG description thus provides a Lagrangian-level realization of CFT, although the existence of the Lagrangian of the latter is not always obvious.

As an example of the LG model, the two-dimensional (2D) $\mathcal{N} = 2$ massless Wess–Zumino (WZ) model (which can be obtained by the dimensional reduction of the four-dimensional WZ model [2]) with a quasi-homogeneous superpotential is considered to give an LG description of the $\mathcal{N} = 2$ superconformal field theory (SCFT) [3–14]. There are various theoretical analyses which support this correspondence [15–24]. It is, however, still difficult to prove this conjecture directly, because the 2D $\mathcal{N} = 2$ massless WZ model is strongly coupled at low energies and perturbation theory suffers from infrared (IR) divergences; the LG description is truly a non-perturbative phenomenon.

A non-perturbative calculational method such as the lattice field theory may provide an alternative approach to this issue. In Ref. [25], the scaling dimension of the scalar field in the IR limit of the 2D $\mathcal{N} = 2$ massless WZ model was measured by using a lattice formulation from Ref. [26]. The case of a single supermultiplet with a cubic superpotential $W = \Phi^3$, which is considered to become the A_2 minimal model in the IR limit, is studied. In Ref. [25], good agreement of the scaling dimension with that of the A_2 model was observed. As is well-recognized, the lattice formulation is in general not compatible with the supersymmetry (SUSY) that must be a crucial element of the above LG correspondence. This is also the

case for the lattice formulation of Ref. [26]. However, the formulation of Ref. [26] exactly preserves one nilpotent SUSY, utilizing the existence of the the Nicolai or Nicolai–Parisi–Sourlas map [27–30].¹ Because of this exactly preserved SUSY, and because this 2D theory is super-renormalizable, it can be argued to all orders of perturbation theory that the full SUSY is automatically restored in the continuum limit.² The study of Ref. [25] thus paved the way for the numerical investigation of the $\mathcal{N} = 2$ LG model, a triumph of the lattice field theory.³

Somewhat later, in Ref. [41], the same $W = \Phi^3$ model was analyzed by using the formulation in Ref. [42]; a similar result on the scaling dimension was obtained. A salient feature of the momentum cutoff formulation of Ref. [42] is that it preserves the full set of SUSY as well as the translational invariance even with a finite cutoff. The formulation is (almost) identical to the dimensional reduction of the lattice formulation [43] of the 4D WZ model on the basis of the SLAC derivative [44, 45]. Although this formulation exactly preserves SUSY, it sacrifices the locality because of the SLAC derivative. See Ref. [46] for an analysis of the issue of the exact SUSY and the locality. Although the SLAC derivative generally suffers from some pathology [47–49], for the 2D $\mathcal{N} = 2$ WZ model it can be argued [42] to all orders of perturbation theory that the locality is automatically restored in the continuum limit. This is precisely because of the exactly preserved SUSY and because this 2D theory is super-renormalizable. Since this formulation preserves the full SUSY, the construction of the associated Noether current, the supercurrent, is straightforward. Then, from the IR limit of the two-point function of the supercurrent, the central charge being fairly consistent with the A_2 model was observed. Thus, this study again supports the conjectured LG correspondence.

In this paper, following on from the study of Ref. [41], we carry out the numerical study of the $\mathcal{N} = 2$ LG model on the basis of the formulation of Ref. [42]. In several aspects we extend and improve the analysis in Ref. [41]. First, we study a higher critical model $W = \Phi^4$, which would correspond to the A_3 minimal model, as well as $W = \Phi^3$ to obtain further support for the LG correspondence and the validity of the formulation. For the scaling dimension, in this paper we use the two-point function in the momentum space instead of the susceptibility of Ref. [41]. Second, the numerical accuracy and the effective number of configurations in the Monte Carlo simulation are quite improved. Third, we also measure the central charge by using the two-point function of the energy–momentum tensor, not only by that of the supercurrent. In Ref. [41], it was reported that the former correlation function was too noisy for extracting the central charge; in the present paper, we avoid this problem by rewriting the correlation function of the energy–momentum tensor by that of the supercurrent by using SUSY Ward–Takahashi (WT) relations. It turns out that after this transformation, the correlation function of the energy–momentum tensor is rather useful to extract the central charge. We also repeat the calculation of the “effective central charge” in Ref. [41] that is an analogue of the Zamolodchikov c -function [50, 51]. All our results below show a coherence picture being consistent with the conjectured LG correspondence.

¹ This feature is common to the lattice formulation of Ref. [31].

² For this issue, see also Refs. [32, 33]. Ref. [34] is a recent review of SUSY on the lattice.

³ References [35–39] are preceding studies on the 2D massive $\mathcal{N} = 2$ WZ model. It appears that the 2D massless $\mathcal{N} = 2$ WZ model is numerically studied in Ref. [40].

In view of the LG/Calabi–Yau correspondence [17, 52–54], we hope that this kind of numerical method will eventually provide a computation method for scattering amplitudes in a superstring theory, whose world sheet theory is given by an $\mathcal{N} = 2$ SCFT but not necessarily by the product of solvable minimal models.

2. Formulation

2.1. The classical action

It is believed that the 2D $\mathcal{N} = 2$ WZ model provides the LG description of the 2D $\mathcal{N} = 2$ SCFT.⁴ The action of the 2D WZ model can be obtained by the dimensional reduction of the 4D $\mathcal{N} = 1$ WZ model [2] whose (Euclidean) action is given by

$$S = \int d^4x d^4\theta \bar{\Phi}\Phi - \int d^4x d^2\theta W(\Phi) - \int d^4x d^2\bar{\theta} W(\bar{\Phi}). \quad (2.1)$$

Here, θ and $\bar{\theta}$ are Grassmann coordinates and Φ is the chiral superfield,

$$\Phi(x, \theta) = A(y) + \sqrt{2} \sum_{\alpha=1}^2 \theta^\alpha \psi_\alpha(y) + \sum_{\alpha=1}^2 \theta^\alpha \theta_\alpha F(y), \quad (2.2)$$

consisting of a complex scalar A , a left-handed spinor ψ , and an auxiliary field F ; the coordinate y is given by

$$y_M = x_M + i \sum_{\alpha=1}^2 \sum_{\dot{\alpha}=\dot{1}}^{\dot{2}} \theta^\alpha \sigma_{M\alpha\dot{\alpha}} \bar{\theta}^{\dot{\alpha}} \quad \text{for } M = 0, 1, 2, 3, \quad (2.3)$$

where σ_0 is the unit matrix and $\sigma_{1,2,3}$ the Pauli matrices. The superpotential $W(\Phi)$ ($W(\bar{\Phi})$) in Eq. (2.1) is assumed to be a polynomial of the superfield Φ ($\bar{\Phi}$).

Under the dimensional reduction, we eliminate the dependence on the coordinates x_2 and x_3 . The coordinates x_0 and x_1 are identified with the 2D coordinates; in what follows, we use the complex coordinates quite often:

$$z \equiv x_0 + ix_1, \quad \bar{z} \equiv x_0 - ix_1. \quad (2.4)$$

The corresponding derivatives are given by

$$\partial \equiv \frac{\partial}{\partial z} = \frac{1}{2}(\partial_0 - i\partial_1), \quad \bar{\partial} \equiv \frac{\partial}{\partial \bar{z}} = \frac{1}{2}(\partial_0 + i\partial_1). \quad (2.5)$$

⁴Here, by $\mathcal{N} = 2$, we mean $\mathcal{N} = (2, 2)$ and not $\mathcal{N} = (2, 0)$.

With these notations,⁵ the Euclidean action of the 2D $\mathcal{N} = 2$ WZ model is given by⁶

$$S = \int d^2x \left[4\partial A^* \bar{\partial} A - F^* F - F^* W'(A)^* - F W'(A) + (\bar{\psi}_1, \psi_2) \begin{pmatrix} 2\partial & W''(A)^* \\ W''(A) & 2\bar{\partial} \end{pmatrix} \begin{pmatrix} \psi_1 \\ \bar{\psi}_2 \end{pmatrix} \right]. \quad (2.8)$$

The basic symmetries of this system, including SUSY, are summarized in Appendix A.

2.2. Momentum cutoff regularization

We quantize the system of Eq. (2.8) by employing a momentum cutoff regularization; this approach is studied in Ref. [42]. As emphasized in Ref. [42], this regularization exactly preserves important symmetries of the system, SUSY and the translational invariance. This is the good news. The bad news is that the regularization breaks the locality. In fact, this formulation is (when the integers L_μ/a are odd implying a spacetime lattice with periodic boundary conditions; see below) nothing but the dimensional reduction of the SUSY-invariant lattice formulation of the 4D WZ model of Ref. [43] that is based on the SLAC derivative [44, 45]. It is well recognized that the SLAC derivative generally suffers from some pathology [47–49]. On the other hand, for the 2D $\mathcal{N} = 2$ WZ model, one can argue to all orders of perturbation theory that the locality is automatically restored when the UV cutoff is removed, thanks to the exactly preserved SUSY [42]. However, since this argument is based on perturbation theory, whose validity for the present *massless* WZ model is not clear due to the IR divergences, strictly speaking, the theoretical basis of our numerical simulation is not quite obvious. Nevertheless, our numerical results below (and those of Ref. [41]) show a coherent picture which strongly suggests the validity of the approach. We want to leave understanding the observed validity of our formulation as a future problem.

Now, let us suppose that the system is defined in a box of physical size $L_0 \times L_1$. The Fourier transformation of each field $\varphi(x)$ in Eq. (2.8) is then defined by

$$\varphi(x) = \frac{1}{L_0 L_1} \sum_p e^{ipx} \varphi(p), \quad \varphi(p) = \int d^2x e^{-ipx} \varphi(x), \quad (2.9)$$

where

$$p_\mu = \frac{2\pi}{L_\mu} n_\mu, \quad (n_\mu = 0, \pm 1, \pm 2, \dots). \quad (2.10)$$

⁵ Defining a two-component Dirac fermion by $\psi \equiv \begin{pmatrix} \psi_1 \\ \bar{\psi}_2 \end{pmatrix}$ and $\bar{\psi}\gamma_0 \equiv (\bar{\psi}_1, \psi_2)$, the 2D Dirac matrices are given by

$$\gamma_0 = \begin{pmatrix} 0 & 1 \\ 1 & 0 \end{pmatrix}, \quad \gamma_1 = \begin{pmatrix} 0 & i \\ -i & 0 \end{pmatrix}, \quad (2.6)$$

that is,

$$\gamma_z = \begin{pmatrix} 0 & 1 \\ 0 & 0 \end{pmatrix}, \quad \gamma_{\bar{z}} = \begin{pmatrix} 0 & 0 \\ 1 & 0 \end{pmatrix}. \quad (2.7)$$

⁶ The Euclidean action of the auxiliary field in the Wess–Zumino model has the “wrong sign”, i.e. the sign is opposite to the Gaussian one. In this sense, the functional integral containing the Euclidean action of the auxiliary field is merely a formal expression. We understand that the auxiliary field is always expressed by using the equation of motion. The functional integral then becomes perfectly well defined under this understanding. Our computation below is based on such a well-defined functional integral.

Note that

$$\varphi^*(p) = \varphi(-p)^*. \quad (2.11)$$

After eliminating the auxiliary field F by the equation of motion, the action in Eq. (2.8) in terms of the Fourier modes yields

$$S = S_B + \frac{1}{L_0 L_1} \sum_p (\bar{\psi}_1, \psi_2)(-p) \begin{pmatrix} 2ip_z & W''(A)^{**} \\ W''(A)^* & 2ip_{\bar{z}} \end{pmatrix} \begin{pmatrix} \psi_1 \\ \bar{\psi}_2 \end{pmatrix}(p), \quad (2.12)$$

where $p_z \equiv (1/2)(p_0 - ip_1)$, $p_{\bar{z}} \equiv (1/2)(p_0 + ip_1)$, $*$ denotes the convolution

$$(\varphi_1 * \varphi_2)(p) \equiv \frac{1}{L_0 L_1} \sum_q \varphi_1(q) \varphi_2(p - q), \quad (2.13)$$

and S_B is the boson part of the action,

$$S_B \equiv \frac{1}{L_0 L_1} \sum_p N^*(-p) N(p), \quad N(p) \equiv 2ip_z A(p) + W'(A)^*(p). \quad (2.14)$$

It is understood that the field product in $W''(A)$ and $W''(A)^*$ is defined by the convolution of Eq. (2.13).

In order to define the functional integral, we then introduce the momentum cutoff Λ and restrict the momentum as

$$|p_\mu| \leq \Lambda \equiv \frac{\pi}{a} \quad \text{for } \mu = 0 \text{ and } 1. \quad (2.15)$$

All dimensionful quantities are measured in units of a . For notational simplicity, we set $a = 1$. With this understanding,

$$p_\mu = \frac{2\pi}{L_\mu} n_\mu, \quad |n_\mu| \leq \frac{L_\mu}{2}. \quad (2.16)$$

We then define the partition function by

$$\mathcal{Z} = \int \prod_{|p_\mu| \leq \pi} \left[dA(p) dA^*(p) \prod_{\alpha=1}^2 d\psi_\alpha(p) \prod_{\dot{\alpha}=\dot{1}}^{\dot{2}} d\bar{\psi}_{\dot{\alpha}}(p) \right] e^{-S}. \quad (2.17)$$

Equation (2.12) is the action in classical theory and thus is invariant under the SUSY transformation and the translation. Since these transformations act on field variables *linearly* (see Appendix A for their explicit form) and do not change the momentum label p , these transformations preserve the restriction on the Fourier modes in Eq. (2.16). As the consequence, our formulation in Eq. (2.17) manifestly preserves these symmetries [42].

2.3. Nicolai map

Our definition of the partition function in the regularized level, Eq. (2.17) of the 2D $\mathcal{N} = 2$ WZ model allows the Nicolai or Nicolai–Parisi–Sourlas map [27–30], which renders the partition function Gaussian integrals [42].⁷ The point is that the Dirac determinant in Eq. (2.17)

⁷This feature is common to the lattice formulation in Refs. [25, 26].

coincides with the Jacobian associated with the change of integration variables from (A, A^*) to (N, N^*) , the variables defined in Eq. (2.14), up to the sign:

$$\det \begin{pmatrix} 2ip_z & W''(A)^{*} \\ W''(A)^{*} & 2ip_{\bar{z}} \end{pmatrix} = \det \frac{\partial(N, N^*)}{\partial(A, A^*)}. \quad (2.18)$$

Hence, after the integration over the fermion fields, the partition function is represented as

$$\begin{aligned} \mathcal{Z} &= \int \prod_{|p_\mu| \leq \pi} [dA(p)dA^*(p)] e^{-S_B} \det \frac{\partial(N, N^*)}{\partial(A, A^*)} \\ &= \int \prod_{|p_\mu| \leq \pi} [dN(p)dN^*(p)] e^{-S_B} \sum_i \text{sign det} \frac{\partial(N, N^*)}{\partial(A, A^*)} \Big|_{A=A_i, A^*=A_i^*}. \end{aligned} \quad (2.19)$$

where A_i ($i = 1, 2, \dots$) are solutions of the set of equations

$$2ip_z A(p) + W'(A)^*(p) - N(p) = 0, \quad p_\mu = \frac{2\pi}{L_\mu} n_\nu, \quad |n_\mu| \leq \frac{L_\mu}{2}, \quad (2.20)$$

and A_i^* are their complex conjugate. Note that, as Eq. (2.14) shows, e^{-S_B} is Gaussian in terms of the variables (N, N^*) ; this is, thus, a drastic simplification.

The representation in Eq. (2.19) thus presents the following simulation algorithm [35] (see also Ref. [55]):

- (1) Generate complex random numbers $N(p)$ for each p_μ in Eq. (2.16) whose real and imaginary parts obey the Gaussian distribution.
- (2) Solve the multi-variable algebraic equations of Eq. (2.20) numerically with respect to A and (ideally) find all the solutions A_i ($i = 1, 2, \dots$).
- (3) Calculate the following sums over solutions:

$$\sum_i \text{sign det} \frac{\partial(N, N^*)}{\partial(A, A^*)} \Big|_{A=A_i, A^*=A_i^*}, \quad (2.21)$$

$$\sum_i \text{sign det} \frac{\partial(N, N^*)}{\partial(A, A^*)} \mathcal{O}(A, A^*) \Big|_{A=A_i, A^*=A_i^*}, \quad (2.22)$$

where \mathcal{O} is an observable of interest. In Appendix B, we present a fast algorithm for the computation of $\text{sign det} \frac{\partial(N, N^*)}{\partial(A, A^*)}$.

- (4) Repeat steps (1)–(3) and compute the averages over configurations of N :

$$\Delta \equiv \left\langle \sum_i \text{sign det} \frac{\partial(N, N^*)}{\partial(A, A^*)} \Big|_{A=A_i, A^*=A_i^*} \right\rangle, \quad (2.23)$$

$$\langle \mathcal{O} \rangle = \frac{1}{\Delta} \left\langle \sum_i \text{sign det} \frac{\partial(N, N^*)}{\partial(A, A^*)} \mathcal{O}(A, A^*) \Big|_{A=A_i, A^*=A_i^*} \right\rangle. \quad (2.24)$$

Here, Δ is the normalized partition function, i.e., the Witten index [56, 57].⁸ If the superpotential W is a polynomial of degree n , we should have $\Delta = n - 1$.⁹

⁸ In our numerical simulations, we find that the statistical error of Δ is much smaller than that of the numerator in the ratio of Eq. (2.24). Hence, we estimate the statistical error of $\langle \mathcal{O} \rangle$ by a simple error-propagation rule in the ratio.

⁹ This can be seen by counting the number of classical vacua.

Since it is easy to generate Gaussian random numbers without any notable autocorrelation, the above algorithm is completely free from any undesired autocorrelation and the critical slowing down; this is a remarkable feature of this algorithm.

Unfortunately, in step (2) we cannot judge whether all the solutions of Eq. (2.20) are found or not because we cannot know a priori the total number of solutions A_i for a given N . The best thing we can do is to collect as many solutions as possible. For this issue, the stability of the number of solutions under the increase of initial trial solutions in the solver algorithm, the agreement of Δ with the expected Witten index and the observation of expected SUSY WT relations provide some consistency checks. In any case, the physical quantities we will compute in what follows, the scaling dimension and the central charge, cannot be free from the systematic error associated with the “undiscovered solutions.” It is difficult to estimate the size of this systematic error at this time and the quoted values of the scaling dimension and the central charge should be taken with this reservation.

3. Simulation setup and classification of configurations

In this paper we consider the 2D WZ model of Eq. (2.8) with the superpotential

$$W(\Phi) = \frac{\lambda}{n} \Phi^n \quad (3.1)$$

with $n = 3$ and 4 , which will be written in the abbreviated forms as $W = \Phi^3$ and $W = \Phi^4$, respectively. We set the coupling constant

$$\lambda = 0.3 \quad (3.2)$$

in units of $a = 1$, as in Refs. [25, 41].

To solve Eq. (2.20) with respect to A , we employ the Newton–Raphson (NR) method.¹⁰ The quality of the obtained configuration A is estimated by the following norm of the residue:

$$\sqrt{\frac{\sum_p |2ip_z A(p) + W'(A)(-p)^* - N(p)|^2}{\sum_q |N(q)|^2}}. \quad (3.3)$$

As we will see below, maximum values of this number are smaller than 10^{-14} for all obtained configurations, and this is much smaller than the corresponding number in Ref. [41].

For a fixed configuration of N , we randomly generate¹¹ initial trial configurations of A so that we obtain 100 solutions for A allowing repetition of identical solutions; this is another improvement compared to the setup of Ref. [41]. A randomly generated initial configuration does not necessarily converge to a solution along the iteration in the NR method; sometimes it diverges and does not provide any solution.¹² Two solutions A_1 and A_2 are regarded as

¹⁰ For the generation of the configurations of N and for the computation of A and $\text{sign det} \frac{\partial(N, N^*)}{\partial(A, A^*)}$ we used a C++ library `Eigen` [58]. In particular, we extensively used the class `PartialPivLU`.

¹¹ The initial value of the real and imaginary parts of $A(p)$ is generated by the Gaussian random number with unit variance as in Ref. [41].

¹² In Ref. [41], the number of *initial trial configurations* is fixed to 100 but we found that this choice sometimes misses some solutions for A , especially for $W = \Phi^4$.

identical if the norm of the difference of the solutions,

$$\sqrt{\frac{\sum_p |A_1(p) - A_2(p)|^2}{\sum_q |A_1(q)|^2}} \quad (3.4)$$

is smaller than 10^{-13} .

For both cases $W = \Phi^3$ and $W = \Phi^4$, for each box size L ,

$$L \equiv L_0 = L_1, \quad (3.5)$$

we generate 640 configurations of N using the Gaussian random number. The box size L is taken as even integers from 8 to 36 for $W = \Phi^3$ and from 8 to 30 for $W = \Phi^4$.

We tabulate the classification of configurations we obtained in Tables 1–3 for $W = \Phi^3$ and in Tables 4–6 for $W = \Phi^4$. The symbols such as $(+++)_2$, for example, imply the following: For a certain configuration of N , we found four solutions A_i ($i = 1, \dots, 4$); sign $\det \frac{\partial(N, N^*)}{\partial(A, A^*)}$ at three of those solutions is positive and negative at one solution. The subscript $2(= 1 + 1 + 1 - 1)$ stands for the contribution of that N configuration to Δ in Eq. (2.23). Table 3, for example, shows that for $L = 36$ we had 13 such configurations of N out of 640 configurations.

In the tables, to indicate the quality of the configurations obtained we list Δ from Eq. (2.23), which should reproduce 2 and 3 for $W = \Phi^3$ and $W = \Phi^4$, respectively. For $W = \Phi^3$, our simulation gives $\Delta = 2$ exactly for all box sizes. For $W = \Phi^4$, Δ deviates from 3 for $L \geq 26$ but only slightly; from this, it might be possible to roughly estimate that the systematic error associated with the solution search (i.e., the possibility that some solutions are missed) is less than 0.5% even for $W = \Phi^4$.

For the same purpose, we also list the one-point function,

$$\delta \equiv \frac{\langle S_B \rangle}{(L_0 + 1)(L_1 + 1)} - 1, \quad (3.6)$$

where S_B is defined in Eq. (2.14), which should identically vanish if the SUSY is exactly preserved [36, 41].¹³

We also show the maximal value of the norm of the residue in Eq. (3.3) and the computation time in core · hour on an Intel Xeon E5 2.0 GHz.

Table 1: Classification of configurations for $W = \Phi^3$.

L	8	10	12	14	16
$(++)_2$	640	640	640	639	639
$(++++)_2$	0	0	0	1	1
Δ	2	2	2	2	2
δ	0.0070(44)	-0.0046(36)	0.0019(30)	-0.0020(25)	-0.0003(23)
core · hour [h]	0.77	2.23	5.5	12.37	25.62

¹³ For the calculation of the one-point function δ and succeeding numerical analyses, we used the programming language `Julia` [59–61].

Table 2: Classification of configurations for $W = \Phi^3$ (continued).

L	18	20	22	24	26
$(++)_2$	634	636	634	637	635
$(++++-)_2$	6	4	6	3	5
Δ	2	2	2	2	2
δ	-0.0000(20)	-0.0015(19)	-0.0006(17)	0.0001(16)	-0.0026(15)
core · hour [h]	48.97	87.03	143.83	236.62	405.28

 Table 3: Classification of configurations for $W = \Phi^3$ (continued).

L	28	30	32	34	36
$(++)_2$	634	626	633	628	627
$(++++-)_2$	6	14	7	12	13
Δ	2	2	2	2	2
δ	-0.0002(13)	0.0000(13)	0.0014(12)	0.0008(11)	0.0007(11)
core · hour [h]	649.78	963.93	1382.07	1936.52	2699.42

 Table 4: Classification of configurations for $W = \Phi^4$.

L	8	10	12	14
$(+++)_3$	638	638	638	638
$(++++-)_3$	2	2	2	2
$(+++++--)_3$	0	0	0	0
$(++++)_4$	0	0	0	0
$(+++++-)_4$	0	0	0	0
$(++)_2$	0	0	0	0
Δ	3	3	3	3
δ	0.0003(45)	0.0035(36)	0.0001(30)	-0.0015(26)
core · hour [h]	3.73	12.8	36.1	89.55

The hot spot in our computation is the LU decomposition involved in the NR method whose computational time scales as $\propto N^3$ for a matrix of size N . Thus, we expect that the computational time scales as $\propto L^6$ as a function of the lattice size L . The actual computational time shown in Fig. 1 is fairly well explained by this theoretical expectation.

4. SUSY Ward–Takahashi relation

As mentioned above, our formulation exactly preserves SUSY even with a finite cutoff. Thus, barring the statistical error and the systematic error associated with the solution search, SUSY WT relations should *hold exactly* for any parameter. The observation of these relations

Table 5: Classification of configurations for $W = \Phi^4$ (continued).

L	16	18	20	22
$(+++)_3$	634	635	632	627
$(++++-)_3$	6	5	6	13
$(+++++--)_3$	0	0	2	0
$(++++)_4$	0	0	0	0
$(+++++-)_4$	0	0	0	0
$(++)_2$	0	0	0	0
Δ	3	3	3	3
δ	0.0006(25)	0.0014(20)	0.0024(20)	0.0023(18)
core · hour [h]	202.65	425.23	872.03	1661.22

Table 6: Classification of configurations for $W = \Phi^4$ (continued).

L	24	26	28	30
$(+++)_3$	625	616	614	615
$(++++-)_3$	15	23	20	22
$(+++++--)_3$	0	0	2	0
$(++++)_4$	0	1	3	2
$(+++++-)_4$	0	0	1	0
$(++)_2$	0	0	0	1
Δ	3	3.002(2)	3.006(3)	3.002(3)
δ	0.0000(16)	0.0004(16)	0.0023(17)	-0.0010(15)
core · hour [h]	2917.48	5004.37	8273.47	12905.13

thus provides a useful check of our simulation and gives a rough idea of the magnitude of the statistical and systematic errors.

The simplest SUSY WT relation is $\delta = 0$ for δ in Eq. (3.6), and in Tables 1–6 we have observed that this relation is reproduced quite well in our simulation. In this section, we present results on two further SUSY WT relations on two-point correlation functions which follow from the identities [41]¹⁴

$$\langle Q_1(A(p)\bar{\psi}_1(-p)) \rangle = 0, \quad (4.1)$$

$$\langle Q_2(F^*(p)\psi_1(-p)) \rangle = 0, \quad (4.2)$$

where the explicit form of the SUSY transformation is given in Appendix A.

First, Eq. (4.1) yields

$$2ip_{\bar{z}} \langle A(p)A^*(-p) \rangle = - \langle \psi_1(p)\bar{\psi}_1(-p) \rangle, \quad (4.3)$$

¹⁴In the present system, SUSY cannot be spontaneously broken because of the non-zero Witten index.

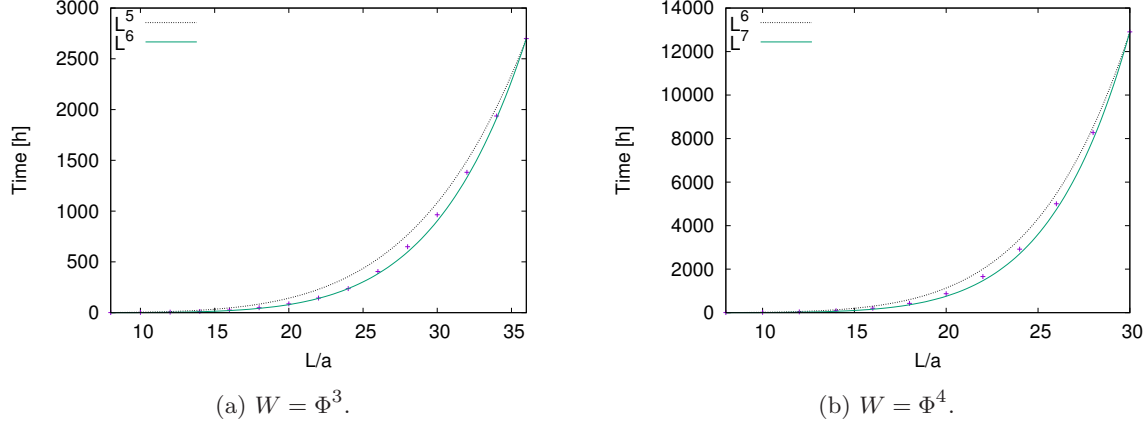


Fig. 1: Computational time as a function of the lattice size.

whose real and imaginary parts are

$$p_1 \langle A(p)A^*(-p) \rangle = \text{Re} \langle \psi_1(p)\bar{\psi}_1(-p) \rangle, \quad (4.4)$$

$$p_0 \langle A(p)A^*(-p) \rangle = -\text{Im} \langle \psi_1(p)\bar{\psi}_1(-p) \rangle. \quad (4.5)$$

In Figs. 2–5 we plot correlation functions in these relations as functions of $-\pi \leq p_0 \leq \pi$. The box size is the maximal one, i.e., $L = 36$ for $W = \Phi^3$ and $L = 30$ for $W = \Phi^4$. The spatial momentum p_1 is fixed to be $p_1 = \pi$ (the largest positive value) or $p_1 = 2\pi/L$ (the smallest positive value). In the figures, the left panel corresponds to the real part relation of Eq. (4.4) and the right one to the imaginary part of Eq. (4.5). In the plots, “bosonic” implies the correlation function on the left-hand side of the WT relation and “fermionic” implies the correlation function on the right-hand side. Errors are statistical only.

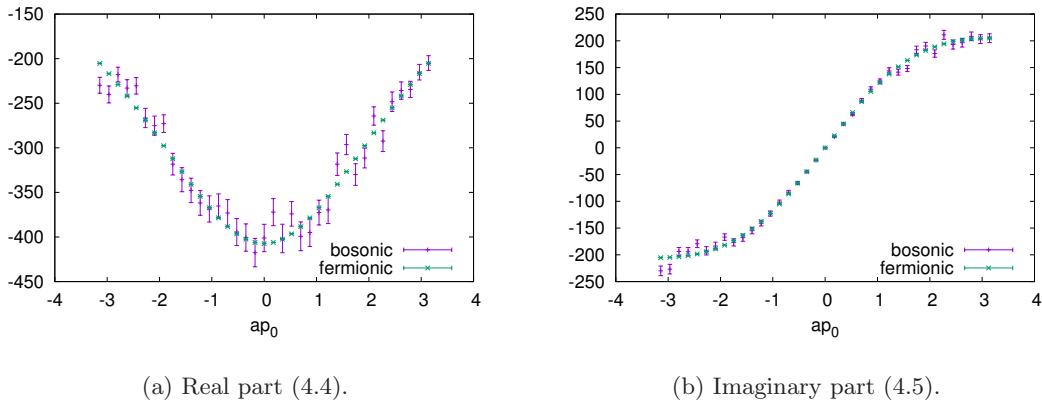
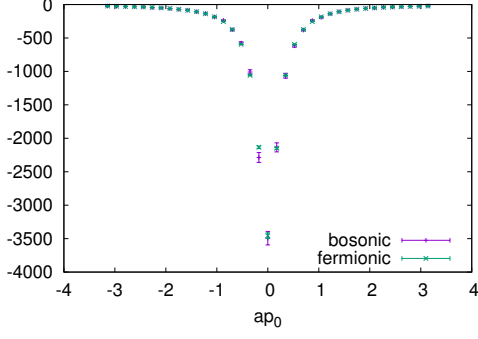


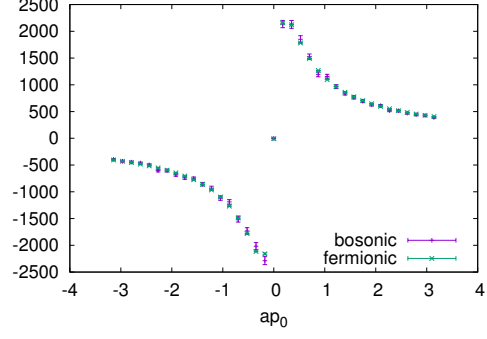
Fig. 2: SUSY WT relation of Eq. (4.3) for $W = \Phi^3$, $L = 36$, and $p_1 = \pi$.

Next, Eq. (4.2) gives the relation

$$\langle F(p)F^*(-p) \rangle = -2ip_z \langle \psi_1(p)\bar{\psi}_1(-p) \rangle, \quad (4.6)$$

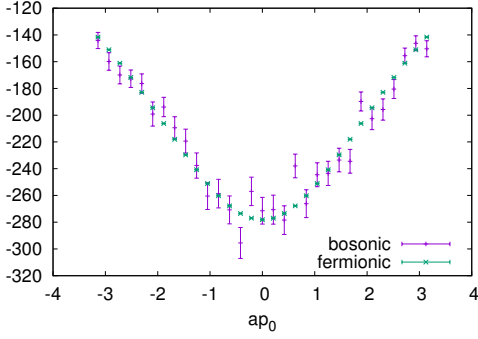


(a) Real part (4.4).

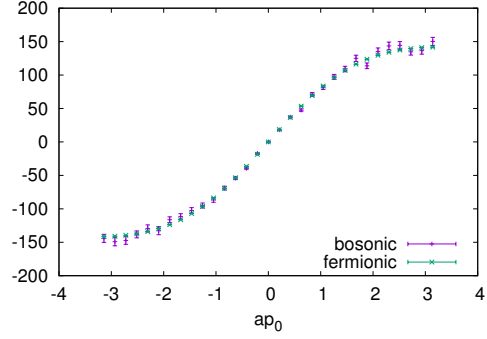


(b) Imaginary part (4.5).

Fig. 3: SUSY WT relation of Eq. (4.3) for $W = \Phi^3$, $L = 36$, and $p_1 = \pi/18$.



(a) Real part (4.4).



(b) Imaginary part (4.5).

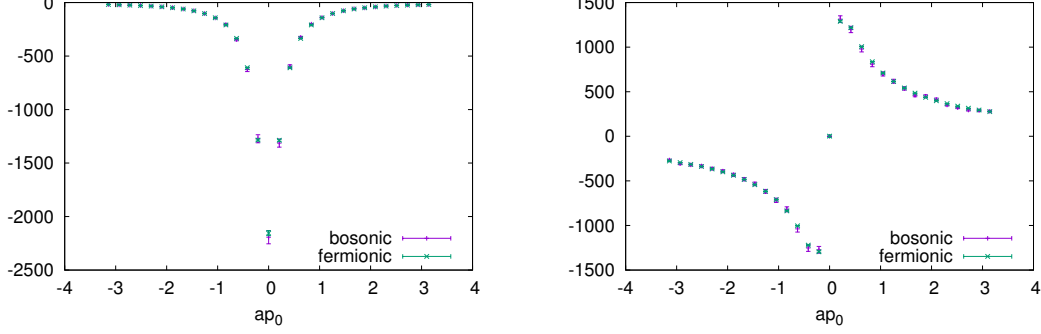
Fig. 4: SUSY WT relation of Eq. (4.3) for $W = \Phi^4$, $L = 30$, and $p_1 = \pi$.

and the real and imaginary parts are given by

$$\langle F(p)F^*(-p) \rangle = -p_1 \operatorname{Re} \langle \psi_1(p) \bar{\psi}_1(-p) \rangle + p_0 \operatorname{Im} \langle \psi_1(p) \bar{\psi}_1(-p) \rangle, \quad (4.7)$$

$$0 = -p_0 \operatorname{Re} \langle \psi_1(p) \bar{\psi}_1(-p) \rangle - p_1 \operatorname{Im} \langle \psi_1(p) \bar{\psi}_1(-p) \rangle. \quad (4.8)$$

In Figs. 6–9 we plot correlation functions in the real part relation of Eq. (4.7); the other conditions and conventions are the same as above. For the computation of the left-hand side



(a) Real part (4.4).

(b) Imaginary part (4.5).

Fig. 5: SUSY WT relation of Eq. (4.3) for $W = \Phi^4$, $L = 30$, and $p_1 = \pi/15$.

of Eq. (4.7) we have used the representation¹⁵

$$\begin{aligned}
\langle F(p)F^*(-p) \rangle &= \langle W'(A)^*(p)W'(A)(-p) \rangle - L_0L_1 \\
&= \left\langle |N(p) - (ip_0 + p_1)A(p)|^2 \right\rangle - L_0L_1.
\end{aligned} \tag{4.12}$$

If the WT relations hold exactly, the “bosonic” points and the “fermionic” points in the plots should coincide with each other. Overall, we observe good agreements within 1σ , as expected. However, there still exist some deviations of order 2σ , especially in the real-part WT relations at the largest spatial momentum $p_1 = \pi$. To argue that these deviations are a result of statistical fluctuations and not due to the omission of some solutions in our solution search, we carried out the measurements corresponding to the left panels of Figs. 2 and 6, respectively but for $L = 8$, by changing the number of configurations by four times, i.e., 640 and 2560. The results are shown in Figs. 10 and 11. We see that although for 640 configurations there exist some discrepancies between the “bosonic” and “fermionic” ones of

¹⁵ A way to derive this relation is to introduce the source term for the auxiliary field:

$$S_J = \frac{1}{L_0L_1} \sum_p [F^*(-p)J(p) + J^*(-p)F(p)]. \tag{4.9}$$

Then, after a (formal) Gaussian integration over the auxiliary field, this term changes to

$$S_J \rightarrow \frac{1}{L_0L_1} \sum_p [-W'(A)(-p)J(p) - J^*(-p)W'(A)^*(p) + J^*(-p)J(p)]. \tag{4.10}$$

Therefore,

$$\begin{aligned}
&\langle F^*(-p)F(p) \rangle \\
&= (L_0L_1)^2 \frac{\delta}{\delta J(p)} \frac{\delta}{\delta J^*(-p)} \\
&\quad \times \left\langle \exp \left\{ \frac{1}{L_0L_1} \sum_q [W'(A)(-q)J^*(q) + J(-q)W'(A)^*(q) - J(-q)J^*(q)] \right\} \right\rangle_{J=0, J^*=0} \\
&= \langle W'(A)^*(p)W'(A)(-p) \rangle - L_0L_1.
\end{aligned} \tag{4.11}$$

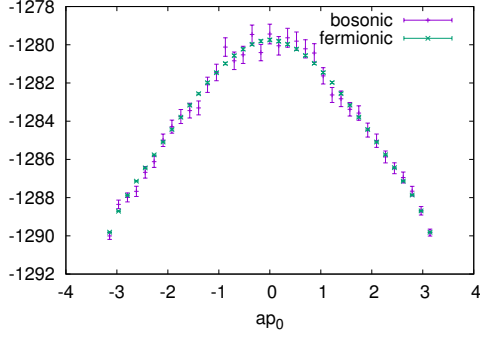


Fig. 6: SUSY WT relation of Eq. (4.7) for $W = \Phi^3$, $L = 36$, and $p_1 = \pi$.

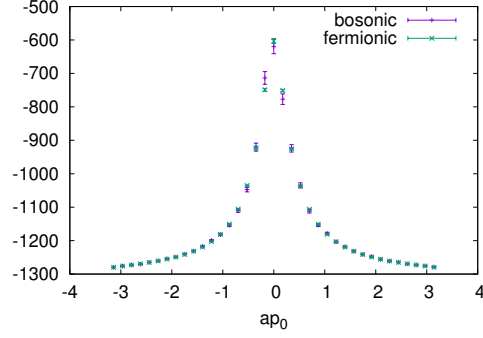


Fig. 7: SUSY WT relation of Eq. (4.7) for $W = \Phi^3$, $L = 36$, and $p_1 = \pi/18$.

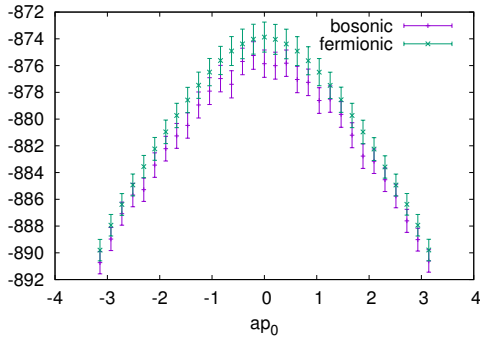


Fig. 8: SUSY WT relation of Eq. (4.7) for $W = \Phi^4$, $L = 30$, and $p_1 = \pi$.

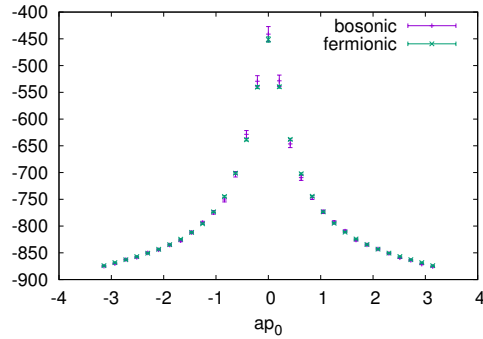


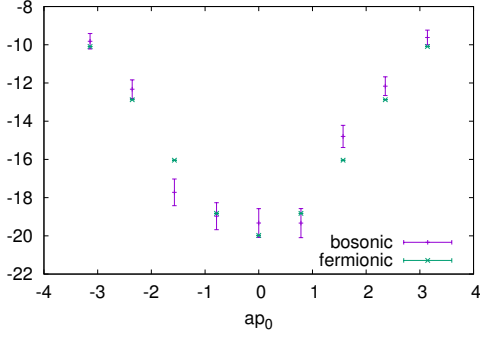
Fig. 9: SUSY WT relation of Eq. (4.7) for $W = \Phi^4$, $L = 30$, and $p_1 = \pi/15$.

order 2σ , when we increase the number of configurations by four times, the statistical error is halved and the discrepancies of the central values actually decrease. From this behavior, we think that the observed discrepancies in the WT relations are due to statistical fluctuations and they eventually disappear as the number of configurations is increased sufficiently.

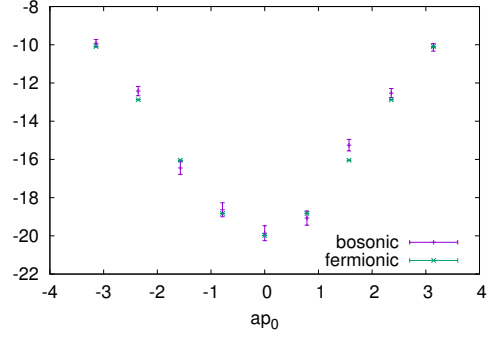
Finally, we mention a general tendency of the statistical error in the correlation functions we found through the numerical simulation. Particularly in the high momentum region, the correlation functions of the scalar field suffer from larger statistical fluctuations than those of the fermion field (as seen in the left panel of Fig. 2). Actually, because of this problem we could not directly examine four-point SUSY WT relations including a four-point correlation function of A and A^* . On the other hand, if we assume the validity of SUSY WT relations, we can use them to rewrite some noisy correlation functions into less noisy ones. This technique will be employed frequently in the following sections.

5. Scaling dimension

In this section, we measure the scaling dimension of the scalar field in the IR limit from the two-point correlation function. If the expected LG correspondence for the WZ model with $W = \Phi^n$ holds, the chiral superfield is identified with the chiral primary field in the

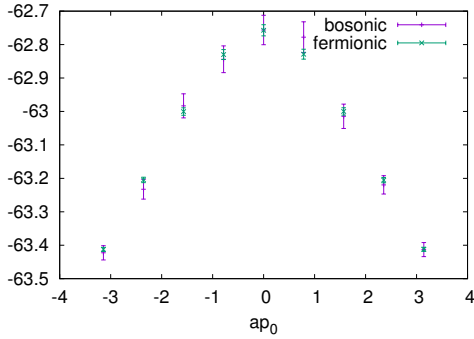


(a) Number of configurations: 640.

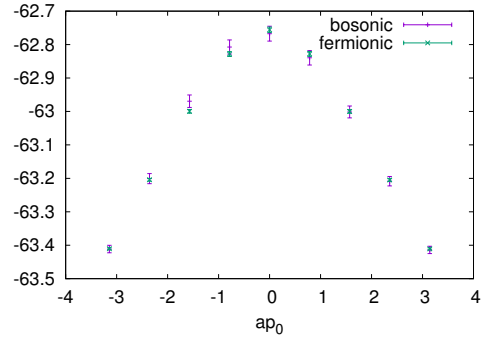


(b) Number of configurations: 2560.

Fig. 10: SUSY WT relation of Eq. (4.4) for $W = \Phi^3$, $L = 8$ and $p_1 = \pi$.



(a) Number of configurations: 640.



(b) Number of configurations: 2560.

Fig. 11: SUSY WT relation of Eq. (4.7) for $W = \Phi^3$, $L = 8$ and $p_1 = \pi$.

A_{n-1} minimal model with the conformal dimension

$$h = \bar{h} = \frac{1}{2n}. \quad (5.1)$$

Thus the two-point function of the scalar field is expected to behave as

$$\langle A(x)A^*(0) \rangle \propto \frac{1}{z^{2h}\bar{z}^{2\bar{h}}}, \quad (5.2)$$

for large $|z|$. To obtain the value of the scaling dimension $h + \bar{h}$, in Ref. [41], the authors computed the susceptibility

$$\chi_\phi \equiv \frac{1}{a^2} \int_{L_0 L_1} d^2x \langle A(x)A^*(0) \rangle. \quad (5.3)$$

To avoid the UV ambiguity at the contact point $x \sim 0$, a small region around $x = 0$ was excised [25]. Then, for the scaling dimension, they obtained

$$1 - h - \bar{h} = 0.616(25)(13). \quad (5.4)$$

The expected value is $1 - h - \bar{h} = 2/3 = 0.666\dots$ for the A_2 minimal model. It turns out, however, that the susceptibility in Eq. (5.3) is quite sensitive to the size of the excised region with the formulation of Ref. [41].

Here, we instead directly study the correlation function in the momentum space $\langle A(p)A^*(-p) \rangle$. The Fourier transformation of Eq. (5.2) reads (assuming $h = \bar{h}$)

$$\langle A(p)A^*(-p) \rangle \propto \frac{1}{(p^2)^{1-h-\bar{h}}}, \quad (5.5)$$

for $|p|$ small.

Also since the SUSY WT relation of Eq. (4.3) shows that

$$\langle \psi_1(p)\bar{\psi}_1(-p) \rangle = -2ip_z \langle A(p)A^*(-p) \rangle \quad (5.6)$$

instead of the two-point function of the scalar field, we may use the two-point function of the fermion field, which is less noisy, as already mentioned.

Figure 12 shows $\ln \langle A(p)A^*(-p) \rangle$ as a function of $\ln p^2$ in the case of the maximal box size, i.e., $L = 36$ for $W = \Phi^3$ and $L = 30$ for $W = \Phi^4$, respectively. We also show the fitting lines in the UV region $\frac{\pi}{\sqrt{2}} \leq |p| < \pi$ and in the IR region $\frac{2\pi}{L} \leq |p| < \frac{4\pi}{L}$. Table 7 summarizes the scaling dimension obtained from the linear fit in the IR region, which is one of our main results in this paper. Recall, however, that those numbers may contain the systematic error associated with the solutions undiscovered by the NR method.

It may be of some interest to see how the values are changed if we do not include a few percent of “strange solutions” in Tables 1–6, such as $(+++)_2$ in Table 1. Thus, we have computed the scaling dimension $1 - h - \bar{h}$ by using only the $(++)_2$ -type solutions for $W = \Phi^3$ ($L = 36$) and the $(+++)_3$ -type solutions for $W = \Phi^4$ ($L = 30$). The result is:

$$1 - h - \bar{h} = 0.6716(82), \quad W = \Phi^3, \quad (5.7)$$

$$1 - h - \bar{h} = 0.7364(83), \quad W = \Phi^4. \quad (5.8)$$

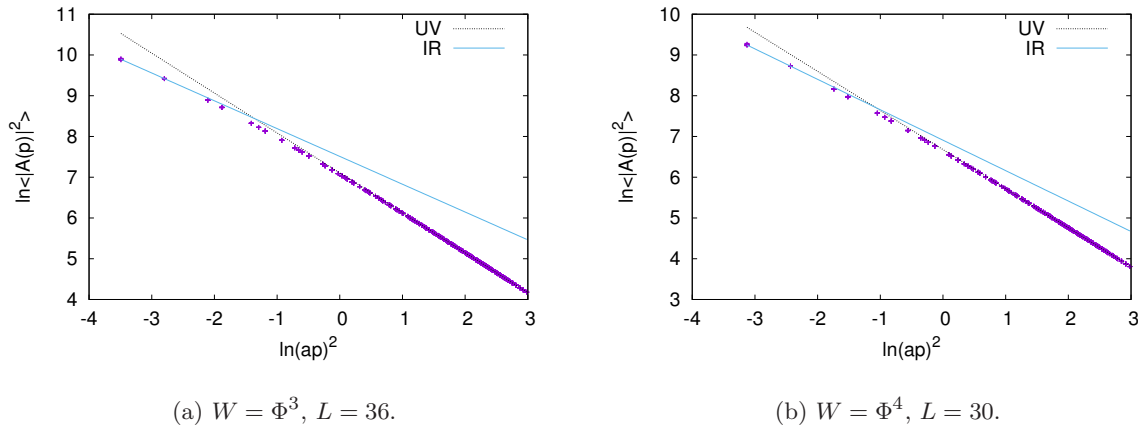


Fig. 12: $\ln \langle A(p)A^*(-p) \rangle$ as a function of $\ln p^2$. The broken and solid lines are linear fits in the UV and IR regions, respectively.

We also plotted in Fig. 13 the scaling dimension obtained by the above method but with different box sizes L . Two horizontal lines show the expected values of $1 - h - \bar{h}$ from the LG correspondence: $1 - h - \bar{h} = 0.666\dots$ for $W = \Phi^3$ and $1 - h - \bar{h} = 0.75$ for $W = \Phi^4$. We clearly see the tendency that the measured scaling dimension approaches the expected

Table 7: Scaling dimensions obtained from the linear fit in the IR region $\frac{2\pi}{L} \leq |p| < \frac{4\pi}{L}$.

W	L	$\chi^2/\text{d.o.f.}$	$1 - h - \bar{h}$	Expected value
Φ^3	36	0.506	0.682(10)(7)	0.666...
Φ^4	30	0.358	0.747(11)(12)	0.75

value as L increases. The approach appears not quite smooth, however, so we do not try any fitting of this plot to extract the $L \rightarrow \infty$ value; we suspect that this non-smoothness is due to statistical fluctuations as we observed for the SUSY WT relation in the previous section.

From the $1 - h - \bar{h}$ case presented in Fig. 13, we estimated the systematic error associated with the finite-volume effect. We estimate it by the maximum deviation of the central values at the three largest volumes; the values obtained in this way are presented in the second parentheses of $1 - h - \bar{h}$ in Table 7.

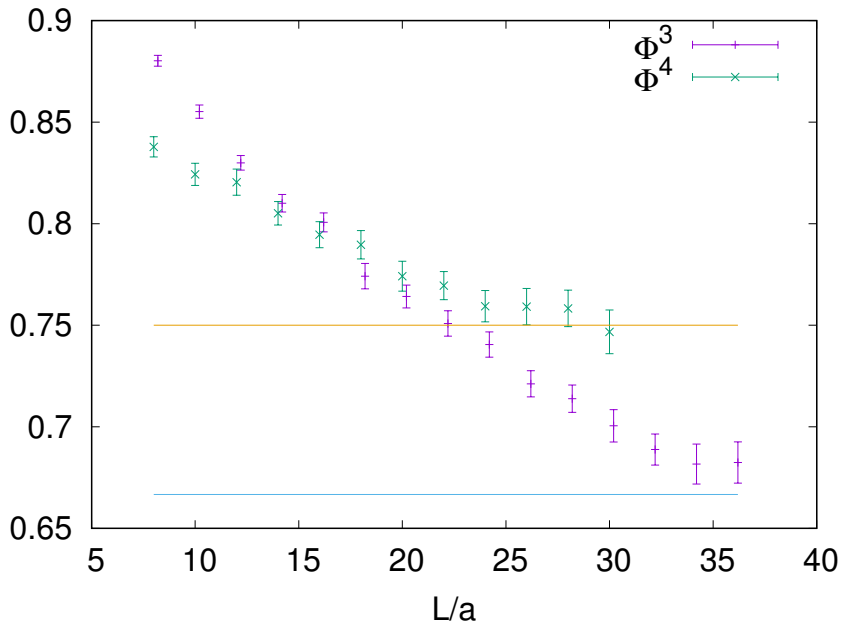


Fig. 13: Scaling dimensions for $W = \Phi^3$ and $W = \Phi^4$ obtained with various box sizes.

It is also interesting to see the “effective scaling dimension” that is obtained from the fitting in some restricted intermediate region of the momentum norm $|p|$. This is shown in Fig. 14. In both panels, the “effective scaling dimension” smoothly changes from that in the IR region (which is summarized in Table 7) and approaches $1 - h - \bar{h} \rightarrow 1$ in the UV limit. This behavior is consistent with the expectation that the 2D $\mathcal{N} = 2$ WZ models become the free $\mathcal{N} = 2$ SCFT in the UV limit, in which the chiral multiplet should have the scaling dimension $1 - h - \bar{h} = 1$.

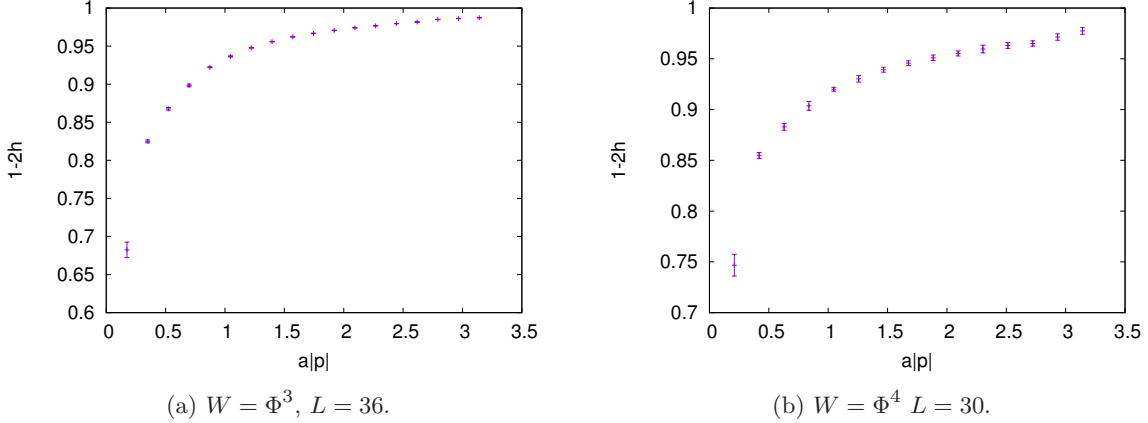


Fig. 14: Scaling dimensions obtained from the linear fitting in various momentum regions from IR to UV, $\frac{2\pi}{L}n \leq |p| < \frac{2\pi}{L}(n+1)$, where $n = 1, \dots, L-1$.

6. Central charge

In this section we consider the measurement of the central charge c , an important quantity that characterizes CFT. This appears, in the first place, in the operator product expansion (OPE) of the energy–momentum tensor,¹⁶

$$T(z)T(0) \sim \frac{c}{2z^4} + \frac{2}{z^2}T(0) + \frac{1}{z}\partial T(0), \quad (6.1)$$

where “ \sim ” implies “ $=$ ” up to non-singular terms. The central charge of the A_n minimal model is

$$c = \frac{3(n-2)}{n} = 1, 1.5, 1.8, \dots, \quad (6.2)$$

for $n = 3, 4, 5, \dots$

From Eq. (6.1), assuming rotational invariance,

$$\langle T(z)T(0) \rangle = \frac{c}{2z^4}. \quad (6.3)$$

Similarly, in $\mathcal{N} = 2$ SCFT, the two-point functions of the supercurrent S^\pm and the $U(1)$ current J are given by

$$\langle S^+(z)S^-(0) \rangle = \frac{2c}{3z^3}, \quad (6.4)$$

$$\langle J(z)J(0) \rangle = \frac{c}{3z^2}. \quad (6.5)$$

Thus, the central charge may also be obtained by computing these two-point functions.

To find the appropriate expression for the supercurrent, the energy–momentum tensor, and the $U(1)$ current such that they form the superconformal multiplet in $\mathcal{N} = 2$ SCFT is itself an intriguing problem, because in our system the $\mathcal{N} = 2$ superconformal symmetry is expected to emerge only in the IR limit. As explained in Appendix A, we adopt the

¹⁶ In this paper we follow the convention of Refs. [62, 63]; this convention is different from that of Ref. [41].

expressions of the former two which become (gamma-) traceless for the free massless WZ model, $W' = 0$. It appears that those expressions work as expected (see also Ref. [41]).

As in the previous section, we numerically compute the correlation function in the momentum space. We consider the two-point functions of the supercurrent, the energy-momentum tensor, and the $U(1)$ current. As we will explain, these two-point functions are related to each other by SUSY, which is an exact symmetry of our formulation. Using this fact, the computation of the whole correlation function can be reduced to that for the supercurrent correlator.

6.1. Central charge from the supercurrent correlator

The argument in Appendix A gives the supercurrent in the momentum space,

$$S^+(p) = S_z^+(p) = \frac{4\pi}{L_0 L_1} \sum_q i(p-q)_z A(p-q) \bar{\psi}_2(q), \quad (6.6)$$

$$S^-(p) = S_z^-(p) = -\frac{4\pi}{L_0 L_1} \sum_q i(p-q)_z A^*(p-q) \psi_2(q). \quad (6.7)$$

We thus compute the two-point function $\langle S^+(p) S^-(p) \rangle$. The Fourier transformation of Eq. (6.4) is, on the other hand,

$$\begin{aligned} \langle S^+(p) S^-(p) \rangle &= L_0 L_1 \int_{L_0 L_1} d^2x e^{-ipx} \langle S^+(x) S^-(0) \rangle \\ &= L_0 L_1 \int_{L_0 L_1} d^2x e^{-ipx} \frac{2c\bar{z}^3}{3(x^2 + \delta^2)^3} \\ &= L_0 L_1 \frac{-i\pi c}{6} \frac{\partial^3}{\partial p_z^3} \left(\frac{|p|}{\delta} \right)^2 K_2(|p|\delta), \end{aligned} \quad (6.8)$$

where we have introduced a regulator δ to tame the singularity at $x = 0$; K_2 is the modified Bessel function of the second kind. Since we are interested in the IR limit, taking the limit $|p|\delta \rightarrow 0$, we have

$$\langle S^+(p) S^-(p) \rangle \rightarrow L_0 L_1 \frac{i\pi c}{3} \frac{p_z^2}{p_{\bar{z}}}. \quad (6.9)$$

We fit the measured two-point function $\langle S^+(p) S^-(p) \rangle$ in the IR region by this function.

We plot the two-point function $\langle S^+(p) S^-(p) \rangle$ in Figs. 15 and 16 for the maximal box size, i.e., $L = 36$ for $W = \Phi^3$ and $L = 30$ for $W = \Phi^4$. In each figure, the left panel is the real part of the correlation function and the right one is the imaginary part. The spatial momentum p_1 is fixed to the positive minimal value, $p_1 = 2\pi/L$. In these figures we also show the function on the right-hand side of Eq. (6.9) with the central charge c obtained from the fit in the IR region $\frac{2\pi}{L} \leq |p| < \frac{4\pi}{L}$; the central charges obtained in this way are tabulated in Table 8. Again, these numbers may contain the systematic error associated with the solutions undiscovered by the NR method.

Compared to the result of Ref. [41] for $W = \Phi^3$,

$$c = 1.09(14)(31), \quad (6.10)$$

the central charge we obtained is somewhat closer to the expected value with the smaller statistical error.

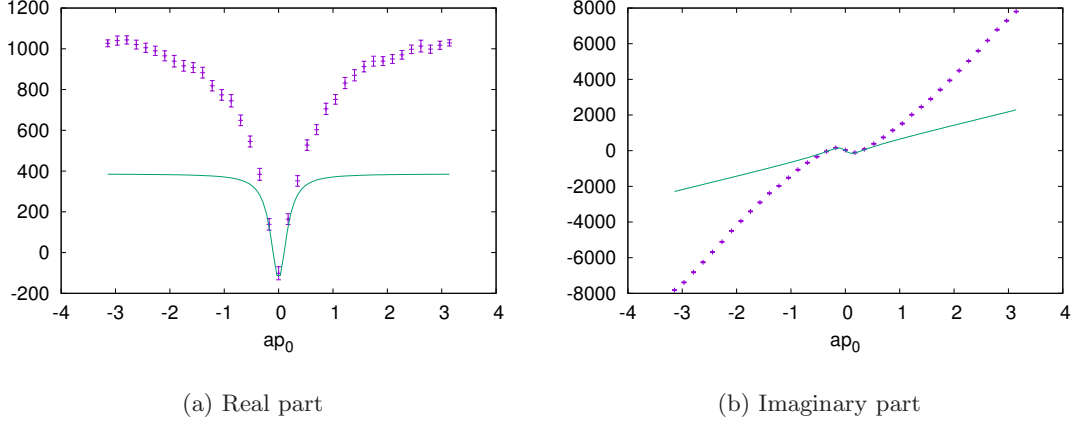


Fig. 15: $\langle S^+(p)S^-(-p) \rangle$ for $W = \Phi^3$, $L = 36$, and $p_1 = \pi/18$. The fitting curves from Eq. (6.9) are also depicted.

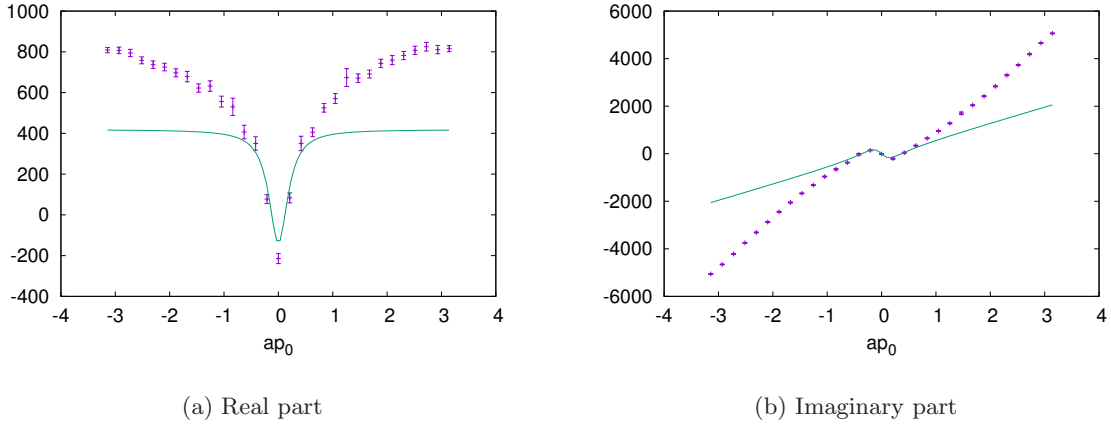


Fig. 16: $\langle S^+(p)S^-(-p) \rangle$ for $W = \Phi^4$, $L = 30$, and $p_1 = \pi/15$. The fitting curves from Eq. (6.9) are also depicted.

Table 8: The central charges obtained from the fit of the supercurrent correlator. The fitting momentum region is $\frac{2\pi}{L} \leq |p| < \frac{4\pi}{L}$.

W	L	$\chi^2/\text{d.o.f.}$	c	Expected value
Φ^3	36	0.928	1.087(68)(56)	1
Φ^4	30	4.606	1.413(65)(31)	1.5

In Fig. 17 we have plotted how the fitted central charge changes as a function of the box size L . From the c presented in Fig. 17, we estimated the systematic error associated with the finite-volume effect. We estimate it by the maximum deviation of central values at the largest three volumes; the values obtained in this way are presented in the second parentheses for c in Table 8.

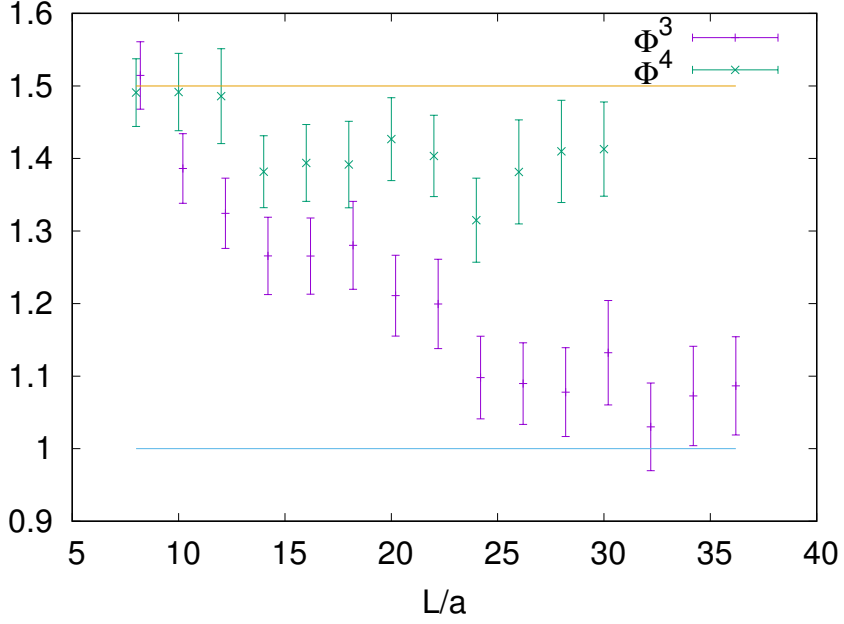


Fig. 17: Central charges obtained by the fit for $W = \Phi^3$ and $W = \Phi^4$ as a function of the box size $L = 8-36$.

As for Fig. 14 in the previous section, it is interesting to see how the central charge obtained by the fit changes as a function of the fitted momentum region [41]. The result is shown in Fig. 18. This “effective central charge” depending on the momentum region is analogous to the supersymmetric version of the Zamolodchikov c -function [50, 51]. As expected, the “effective central charge” changes from the IR value to $c = 3$ in the UV limit in which the system is expected to become a free $\mathcal{N} = 2$ SCFT.

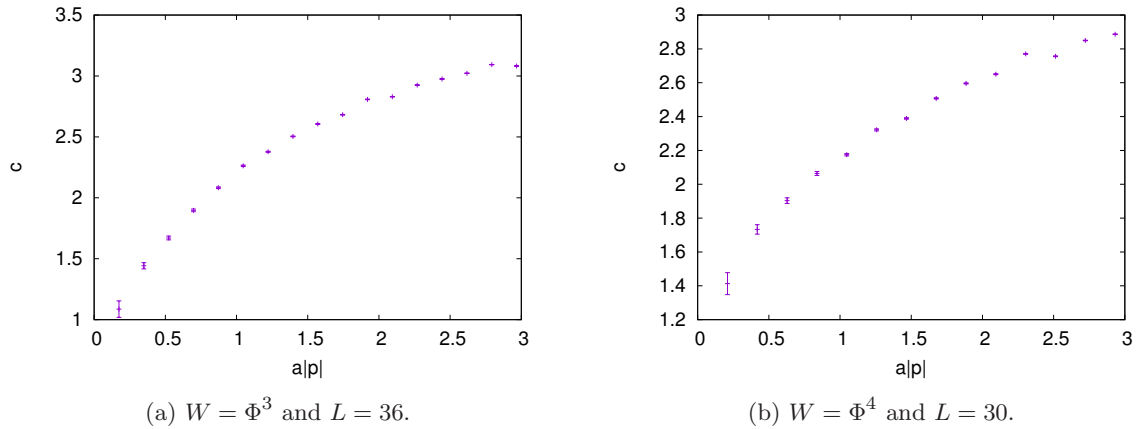


Fig. 18: “Effective central charge” obtained by the fit in various momentum regions, $\frac{2\pi}{L}n \leq |p| < \frac{2\pi}{L}(n+1)$ ($n = 1, \dots, L-1$).

6.2. Central charge from the energy–momentum tensor correlator

As discussed in Appendix A, the energy–momentum tensor $T = T_{zz}$, which is expected to be consistent with the conformal symmetry, is given in the momentum space by

$$T(p) = \frac{\pi}{L_0 L_1} \sum_q \left[4(p-q)_z q_z A^*(p-q) A(q) - i q_z \psi_2(p-q) \bar{\psi}_2(q) + i(p-q)_z \psi_2(p-q) \bar{\psi}_2(q) \right]. \quad (6.11)$$

It turns out that this expression as it stands leads to a very noisy two-point correlation function. Fortunately, noting the fact that the energy–momentum tensor of Eq. (6.11) is the SUSY transformation of the supercurrent in Eqs. (6.6) and (6.7),

$$T(p) = \frac{1}{4} Q_2 S^+(p) - \frac{1}{4} \bar{Q}_2 S^-(p), \quad (6.12)$$

where the SUSY transformation is given in Appendix A, we can express the two-point function of the energy–momentum tensor by a linear combination of two-point functions of the supercurrent which are less noisy:

$$\langle T(p) T(-p) \rangle = -\frac{2ip_z}{16} \langle S^+(p) S^-(p) + S^-(p) S^+(p) \rangle. \quad (6.13)$$

Note that this relation holds exactly in our formulation that preserves SUSY.

The Fourier transformation of Eq. (6.3) is, by the same procedure as Eqs. (6.8) and (6.9),

$$\begin{aligned} \langle T(p) T(-p) \rangle &= L_0 L_1 \frac{\pi c}{2 \cdot 4!} \frac{\partial^4}{\partial p_z^4} \left(\frac{|p|}{\delta} \right)^3 K_3(|p|\delta) \\ &\rightarrow L_0 L_1 \frac{\pi c p_z^3}{12 p_{\bar{z}}}. \end{aligned} \quad (6.14)$$

We plot the two-point function $\langle T(p) T(-p) \rangle$ of Eq. (6.13) in Figs. 19 and 20 for the maximal box size, i.e., $L = 36$ for $W = \Phi^3$ and $L = 30$ for $W = \Phi^4$. In each figure, the left panel is the real part of the correlation function and the right one is the imaginary part. The spatial momentum p_1 is fixed to the positive minimal value, $p_1 = 2\pi/L$. In these figures we also show the function in Eq. (6.14) with the central charge c obtained from the fit in the IR region $\frac{2\pi}{L} \leq |p| < \frac{4\pi}{L}$. The central charges obtained in this way are tabulated in Table 9; this is another main result of this paper. Recall again, however, that these numbers may contain the systematic error associated with the solutions undiscovered by the NR method.

Table 9: The central charges obtained from the fit of the energy–momentum tensor correlator. The fitting momentum region is $\frac{2\pi}{L} \leq |p| < \frac{4\pi}{L}$.

W	L	$\chi^2/\text{d.o.f.}$	c	Expected value
Φ^3	36	1.017	1.061(36)(34)	1
Φ^4	30	0.916	1.415(36)(36)	1.5

We repeated the computation of the central charge c by using only the $(++)_2$ -type solutions for $W = \Phi^3$ ($L = 36$) and the $(+++)_3$ -type solutions for $W = \Phi^4$ ($L = 30$), to see how the

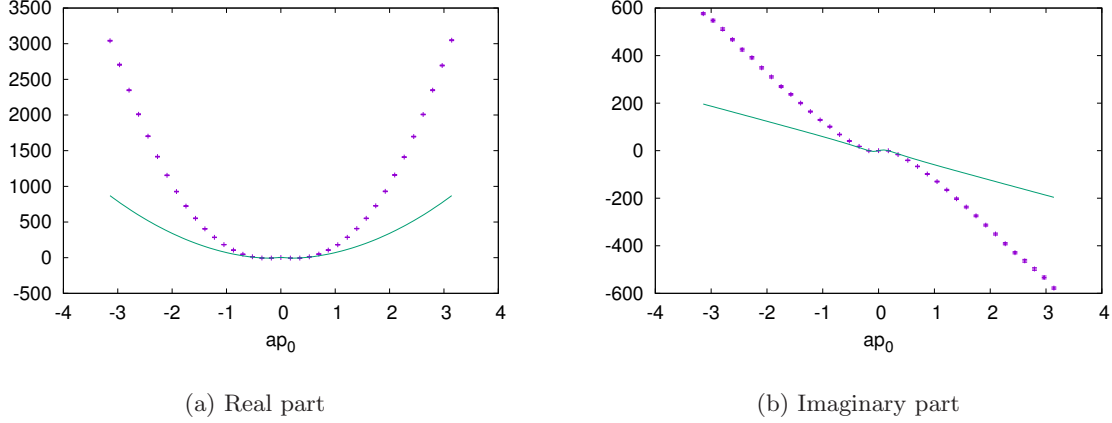


Fig. 19: $\langle T(p)T(-p) \rangle$ for $W = \Phi^3$, $L = 36$, and $p_1 = \pi/18$. The fitting curve of Eq. (6.14) is also depicted.

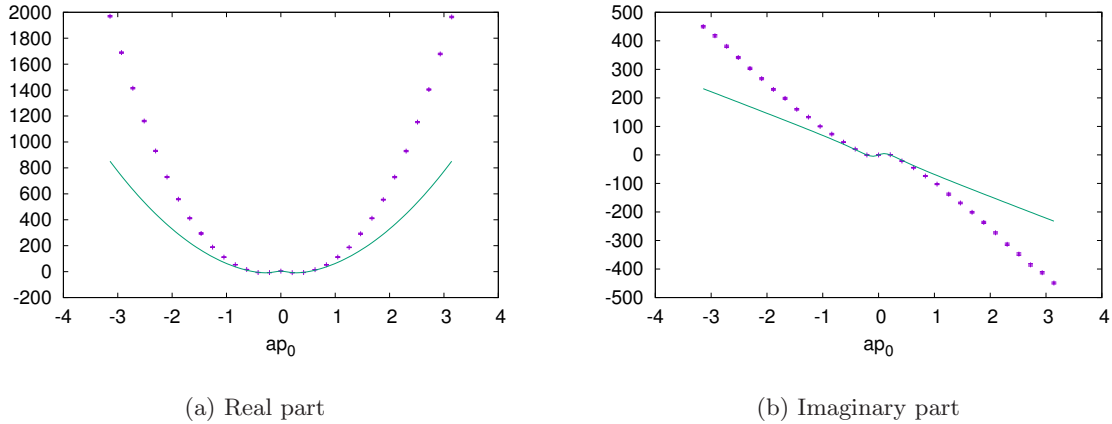


Fig. 20: $\langle T(p)T(-p) \rangle$ for $W = \Phi^4$, $L = 36$, and $p_1 = \pi/15$. The fitting curve by Eq. (6.14) is also depicted.

values are changed if we do not include a few percent “strange solutions.” The results are:

$$c = 1.057(34) \quad (W = \Phi^3), \quad (6.15)$$

$$c = 1.288(28) \quad (W = \Phi^4). \quad (6.16)$$

One may note that the fit in Table 9 is better than that in Table 8, in the sense that $\chi^2/\text{d.o.f.}$ is very close to 1 in the former. This is due to the fact that the real and imaginary parts of the two-point correlation function of Eq. (6.13) are exactly (anti-)symmetric under $p \rightarrow -p$, while the numerical data of $\langle S^+(p)S^-(-p) \rangle$ itself does not possess this property.¹⁷ The number of data points is thus effectively doubled.

¹⁷ This (anti-)symmetry under $p \rightarrow -p$ is fulfilled within the margin of the statistical error; one may also (anti-)symmetrize the two-point function $\langle S^+(p)S^-(-p) \rangle$ by hand.

In Fig. 21, we plotted how the fitted central charge changes as a function of the box size L . From c presented in Fig. 21, we again estimated the systematic error associated with the finite-volume effect. The values obtained in this way are presented in the second parentheses for c in Table 9.

Also, in Fig. 22 the “effective central charge” obtained from the fit in various momentum regions is depicted; from IR to UV, it again shows the expected behavior analogously to the Zamolodchikov c -function.

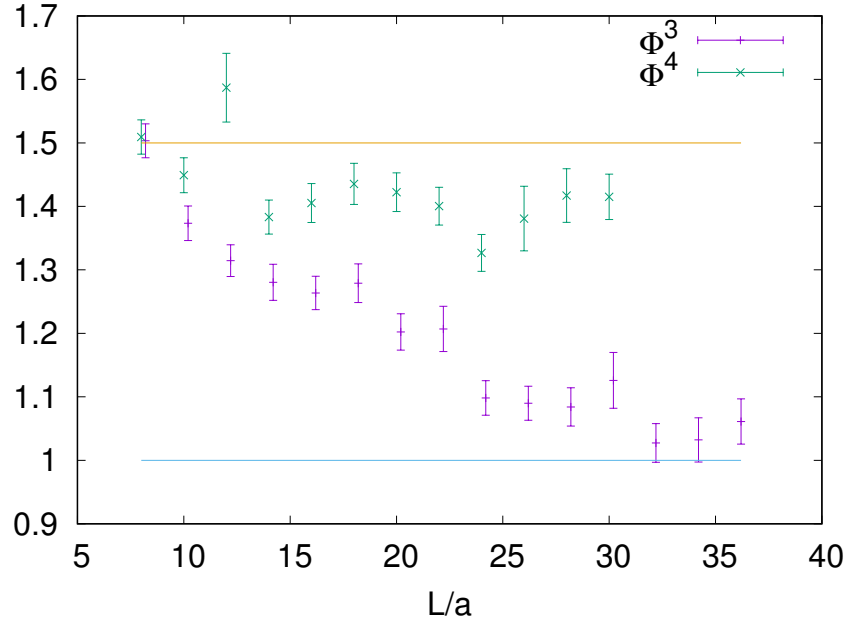


Fig. 21: Central charges obtained by the fit for $W = \Phi^3$ and $W = \Phi^4$ as a function of the box size $L = 8$ –36.

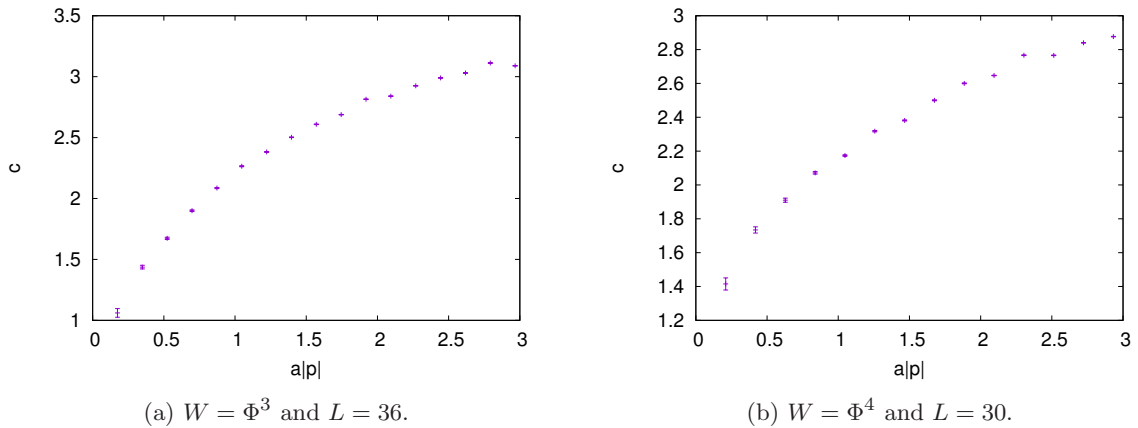


Fig. 22: “Effective central charge” obtained by the fit in various momentum regions, $\frac{2\pi}{L}n \leq |p| < \frac{2\pi}{L}(n+1)$ ($n = 1, \dots, L-1$).

6.3. Central charge from the $U(1)$ current correlator

Finally, we consider the $U(1)$ current correlator. As discussed in Appendix A, the $U(1)$ current is given by

$$J(p) = \frac{2\pi}{L_0 L_1} \sum_q \bar{\psi}_2(p-q) \psi_2(q). \quad (6.17)$$

The two-point function of this current is expected to behave in the IR limit as

$$\begin{aligned} \langle J(p) J(-p) \rangle &= L_0 L_1 \frac{-\pi c}{3} \frac{\partial^2}{\partial p_z^2} \frac{|p|}{\delta} K_1(|p|\delta) \\ &\rightarrow L_0 L_1 \frac{-\pi c}{3} \frac{p_z}{p_z}. \end{aligned} \quad (6.18)$$

We note that the supercurrent S^\pm can be rewritten as the SUSY transformation of J ,

$$S^+(p) = \bar{Q}_2 J(p), \quad S^-(p) = Q_2 J(p). \quad (6.19)$$

Therefore,

$$\langle S^+(p) S^-(p) + S^-(p) S^+(p) \rangle = -2ip_z \langle J(p) J(-p) \rangle. \quad (6.20)$$

This shows that the computation of the $U(1)$ current correlator is identical to the energy-momentum tensor correlator of Eq. (6.13) up to a proportionality factor. We expect that we would obtain almost the same results as the previous subsection, so we do not carry out the analysis on this correlator.

7. Conclusion

In this paper, following on from the study of Ref. [41], we numerically studied the IR behavior of the 2D $\mathcal{N} = 2$ WZ model with the superpotentials $W = \Phi^3$ and $W = \Phi^4$. We used the SUSY-invariant momentum-cutoff formulation which allows, because of exact symmetries, a straightforward construction of the Noether currents, i.e., the supercurrent and the energy-momentum tensor. The simulation algorithm is free from autocorrelation because it utilizes the Nicolai map. From two-point correlation functions in the momentum space, we determined the scaling dimension of the scalar field (Table 7) and the central charge (Table 9) in the IR region. It appears that these results, with the flow of the “effective central charge” in Fig. 22, are consistent with the conjectured LG correspondence to the A_2 and A_3 minimal SCFT.¹⁸

As future prospects, we may further extend the present study to WZ models with multiple superfields and more complicated superpotentials such as the ADE-type theories in Table 10 [16] (the results of the present paper apply to the A_2 , A_3 , and E_6 models).

For a possible application of the present calculational method to the superstring compactification to the Calabi–Yau quintic threefold, the simulation of the $W = \Phi^5$ model will be an important starting point. We are now considering various possible extensions of the present study.

¹⁸ Although those numbers may contain the systematic error associated with the solutions undiscovered by the NR method.

Table 10: ADE-type theories

Algebra	Superpotential W	Central charge c
A_n	$\Phi^{n+1}, n \geq 1$	$3 - 6/(n + 1)$
D_n	$\Phi^{n-1} + \Phi\Phi'^2, n \geq 3$	$3 - 6/2(n - 1)$
E_6	$\Phi^3 + \Phi'^4$	$3 - 6/12$
E_7	$\Phi^3 + \Phi\Phi'^3$	$3 - 6/18$
E_8	$\Phi^3 + \Phi'^5$	$3 - 6/30$

Acknowledgments

We would like to thank Katsumasa Nakayama and Hisao Suzuki for helpful suggestions and discussions. This work was supported by JSPS Grant-in-Aid for Scientific Research Grant Numbers JP18J20935 (O. M.) and JP16H03982 (H. S.).

A. Symmetries and the Noether currents

In this Appendix we summarize basic symmetries of the 2D $\mathcal{N} = 2$ WZ model, i.e., SUSY, the translation, and the $U(1)$ symmetry and the associated Noether currents, the supercurrent, the energy-momentum tensor, and the $U(1)$ current. The explicit form of the former two Noether currents is ambiguous because of freedom to add a divergence-free term and/or a term that is proportional to the equation of motion. We remove such ambiguity by imposing that they are (gamma-) traceless for the *massless free WZ model*. This is a natural requirement because the massless free WZ model itself is an $\mathcal{N} = 2$ SCFT which possesses the $\mathcal{N} = 2$ superconformal symmetry.

A.1. SUSY and the supercurrent

The SUSY transformation in the 2D $\mathcal{N} = 2$ WZ model consists of four spinor components, Q_α ($\alpha = 1, 2$) and $\bar{Q}_{\dot{\alpha}}$ ($\dot{\alpha} = \dot{1}, \dot{2}$). Q_α is defined by

$$Q_1 \bar{\psi}_1(x) = -2\bar{\partial}A^*(x), \quad Q_1 A^*(x) = 0, \quad (\text{A1})$$

$$Q_1 F^*(x) = 2\bar{\partial}\bar{\psi}_2(x), \quad Q_1 \bar{\psi}_2(x) = 0, \quad (\text{A2})$$

$$Q_1 A(x) = \psi_1(x), \quad Q_1 \psi_1(x) = 0, \quad (\text{A3})$$

$$Q_1 \psi_2(x) = F(x), \quad Q_1 F(x) = 0, \quad (\text{A4})$$

and

$$Q_2 \bar{\psi}_2(x) = -2\partial A^*(x), \quad Q_2 A^*(x) = 0, \quad (\text{A5})$$

$$Q_2 F^*(x) = -2\partial\bar{\psi}_1(x), \quad Q_2 \bar{\psi}_1(x) = 0, \quad (\text{A6})$$

$$Q_2 A(x) = \psi_2(x), \quad Q_2 \psi_2(x) = 0, \quad (\text{A7})$$

$$Q_2 \psi_1(x) = -F(x), \quad Q_2 F(x) = 0. \quad (\text{A8})$$

$\bar{Q}_{\dot{\alpha}}$ is, on the other hand, defined by

$$\bar{Q}_{\dot{1}}\psi_1(x) = -2\bar{\partial}A(x), \quad \bar{Q}_{\dot{1}}A(x) = 0, \quad (\text{A9})$$

$$\bar{Q}_{\dot{1}}F(x) = -2\bar{\partial}\psi_2(x), \quad \bar{Q}_{\dot{1}}\psi_2(x) = 0, \quad (\text{A10})$$

$$\bar{Q}_{\dot{1}}A^*(x) = \bar{\psi}_1(x), \quad \bar{Q}_{\dot{1}}\bar{\psi}_1(x) = 0, \quad (\text{A11})$$

$$\bar{Q}_{\dot{1}}\bar{\psi}_2(x) = -F^*(x), \quad \bar{Q}_{\dot{1}}F^*(x) = 0, \quad (\text{A12})$$

and

$$\bar{Q}_{\dot{2}}\psi_2(x) = -2\partial A(x), \quad \bar{Q}_{\dot{2}}A(x) = 0, \quad (\text{A13})$$

$$\bar{Q}_{\dot{2}}F(x) = 2\partial\psi_1(x), \quad \bar{Q}_{\dot{2}}\psi_1(x) = 0, \quad (\text{A14})$$

$$\bar{Q}_{\dot{2}}A^*(x) = \bar{\psi}_2(x), \quad \bar{Q}_{\dot{2}}\bar{\psi}_2(x) = 0, \quad (\text{A15})$$

$$\bar{Q}_{\dot{2}}\bar{\psi}_1(x) = F^*(x), \quad \bar{Q}_{\dot{2}}F^*(x) = 0. \quad (\text{A16})$$

We see that these transformations fulfill simple anti-commutation relations,

$$\{Q_1, \bar{Q}_{\dot{1}}\} = -2\bar{\partial}, \quad (\text{A17})$$

$$\{Q_2, \bar{Q}_{\dot{2}}\} = -2\partial, \quad (\text{A18})$$

$$\{Q_1, \bar{Q}_{\dot{2}}\} = \{Q_2, \bar{Q}_{\dot{1}}\} = 0, \quad (\text{A19})$$

$$\{Q_\alpha, Q_\beta\} = \{\bar{Q}_{\dot{\alpha}}, \bar{Q}_{\dot{\beta}}\} = 0. \quad (\text{A20})$$

The supercurrent, the Noether current associated with SUSY can be read off by considering the localized SUSY transformation in the action. That is, under

$$\delta\varphi(x) = \sum_{\alpha=1}^2 \xi^\alpha(x) Q_\alpha \varphi(x) - \sum_{\dot{\alpha}=\dot{1}}^{\dot{2}} \bar{\xi}^{\dot{\alpha}}(x) \bar{Q}_{\dot{\alpha}} \varphi(x), \quad (\text{A21})$$

where φ stands for a generic field and $\xi^\alpha(x)$ and $\bar{\xi}^{\dot{\alpha}}(x)$ are localized Grassmann parameters, the action changes as

$$\delta S = \frac{1}{2\pi} \int d^2x \sum_{\mu} \left[\xi^1(x) \partial_{\mu} \bar{S}_{\mu}^{+}(x) + \xi^2(x) \partial_{\mu} S_{\mu}^{-}(x) + \bar{\xi}^{\dot{1}}(x) \partial_{\mu} \bar{S}_{\mu}^{-}(x) + \bar{\xi}^{\dot{2}}(x) \partial_{\mu} S_{\mu}^{+}(x) \right]. \quad (\text{A22})$$

Here, superscripts \pm denote the $U(1)$ charge ± 1 , which will be defined in Sect. A.3 below. The definition of the supercurrent S_{μ}^{\pm} is still ambiguous because of the freedom to add a divergence-free term and/or a term that is proportional to the equation of motion. We can remove the ambiguity [41] by imposing the gamma-traceless condition,

$$\sum_{\mu} \gamma_{\mu} \begin{pmatrix} \bar{S}_{\mu}^{\pm} \\ S_{\mu}^{\pm} \end{pmatrix} = 0, \quad (\text{A23})$$

that is,

$$S_{\bar{z}}^{\pm} = \bar{S}_{\bar{z}}^{\pm} = 0, \quad (\text{A24})$$

for the massless free WZ model, $W' = 0$.

Calculating the above variation and imposing Eq. (A24), we have [41]

$$S_z^+ = 4\pi\bar{\psi}_2\partial A, \quad S_{\bar{z}}^+ = 2\pi\psi_1 W'(A), \quad (\text{A25})$$

$$S_z^- = -4\pi\psi_2\partial A^*, \quad S_{\bar{z}}^- = 2\pi\bar{\psi}_1 W'(A)^*, \quad (\text{A26})$$

$$\bar{S}_z^+ = -2\pi\bar{\psi}_2 W'(A)^*, \quad \bar{S}_{\bar{z}}^+ = -4\pi\psi_1 \bar{\partial} A^*, \quad (\text{A27})$$

$$\bar{S}_z^- = -2\pi\psi_2 W'(A), \quad \bar{S}_{\bar{z}}^- = 4\pi\bar{\psi}_1 \bar{\partial} A. \quad (\text{A28})$$

A.2. Translational invariance and the energy–momentum tensor

The energy–momentum tensor is the Noether current associated with the translational invariance. To remove its ambiguity, we require the traceless condition

$$\sum_{\mu} T_{\mu\mu} = 0, \quad (\text{A29})$$

that is,

$$T_{z\bar{z}} = T_{\bar{z}z} = 0, \quad (\text{A30})$$

for the massless free WZ model, $W' = 0$.

The energy–momentum tensor, however, has wider ambiguity than the supercurrent and, because of this, it is difficult to find the energy–momentum tensor which fulfills the above requirement if we simply follow the above procedure, i.e., starting from the variation of the action under the localized translation and then imposing the traceless condition.

A better strategy is the following: We consider the infinitesimal transformation of the form

$$\delta A(x) = - \sum_{\mu} v_{\mu} \partial_{\mu} A(x), \quad (\text{A31})$$

$$\delta\psi_1(x) = - \sum_{\mu} v_{\mu} \partial_{\mu} \psi_1(x) - \frac{1}{2}(\bar{\partial}v_{\bar{z}})\psi_1(x), \quad (\text{A32})$$

$$\delta\bar{\psi}_1(x) = - \sum_{\mu} v_{\mu} \partial_{\mu} \bar{\psi}_1(x) - \frac{1}{2}(\partial v_z)\bar{\psi}_1(x), \quad (\text{A33})$$

$$\delta\psi_2(x) = - \sum_{\mu} v_{\mu} \partial_{\mu} \psi_2(x) - \frac{1}{2}(\partial v_z)\psi_2(x), \quad (\text{A34})$$

$$\delta\bar{\psi}_2(x) = - \sum_{\mu} v_{\mu} \partial_{\mu} \bar{\psi}_2(x) - \frac{1}{2}(\partial v_z)\bar{\psi}_2(x), \quad (\text{A35})$$

$$\delta F(x) = - \sum_{\mu} v_{\mu} \partial_{\mu} F(x). \quad (\text{A36})$$

When the parameter v_{μ} is constant, this is simply the translation that is a symmetry of the WZ model. When $v_{\mu} \propto \epsilon_{\mu\nu}x_{\nu}$, this is the infinitesimal Lorentz transformation that is also a symmetry of the WZ model. Thus, localizing the parameter v_{μ} as $v_{\mu}(x)$, the variation of the action gives rise to a conserved current. By construction, this current is a combination of the canonical energy–momentum tensor, the Lorentz current, and the equation of motion. Moreover, when the parameters v_z and $v_{\bar{z}}$ are holomorphic and anti-holomorphic, respectively, $v_z = v_z(z)$ and $v_{\bar{z}} = v_{\bar{z}}(\bar{z})$, then Eqs. (A31)–(A36) coincide with the conformal transformation, that is an exact invariance of the massless free WZ model. As a consequence, when

$W' = 0$ the conserved Noether current obtained by localizing v_μ as $v_\mu(x)$ must generate the conformal symmetry, i.e., it must be related to the traceless energy–momentum tensor.

In this way, from the variation of the action under Eqs. (A31)–(A36),

$$\delta S = -\frac{1}{2\pi} \int d^2x \sum_{\mu\nu} v_\nu(x) \partial_\mu T_{\mu\nu}(x), \quad (\text{A37})$$

we have

$$\begin{aligned} T_{\mu\nu} = & -2\pi \partial_\mu A^* \partial_\nu A - 2\pi \partial_\nu A^* \partial_\mu A \\ & + \pi \delta_{\mu\nu} [2\partial_\rho A^* \partial_\rho A - 2F^* F - 2F^* W'(A)^* - 2FW'(A) \\ & \quad + W''(A)^* \bar{\psi}_1 \bar{\psi}_2 + W''(A) \psi_2 \psi_1] \\ & - \pi (\delta_{0\mu} - i\delta_{1\mu}) (\delta_{0\nu} - i\delta_{1\nu}) (\bar{\psi}_1 \bar{\partial} \psi_1 - \bar{\partial} \bar{\psi}_1 \psi_1) \\ & - \pi (\delta_{0\mu} + i\delta_{1\mu}) (\delta_{0\nu} + i\delta_{1\nu}) (\psi_2 \partial \bar{\psi}_2 - \partial \psi_2 \bar{\psi}_2). \end{aligned} \quad (\text{A38})$$

This can be written as

$$T(\equiv T_{zz}) = -4\pi \partial A^* \partial A - \pi \psi_2 \partial \bar{\psi}_2 + \pi \partial \psi_2 \bar{\psi}_2, \quad (\text{A39})$$

$$\bar{T}(\equiv T_{\bar{z}\bar{z}}) = -4\pi \bar{\partial} A^* \bar{\partial} A^* - \pi \bar{\psi}_1 \bar{\partial} \psi_1 + \pi \bar{\partial} \bar{\psi}_1 \psi_1, \quad (\text{A40})$$

$$T_{z\bar{z}} = T_{\bar{z}z} = -\pi F^* F - \pi F^* W'(A)^* - \pi FW'(A) + \frac{\pi}{2} W''(A)^* \bar{\psi}_1 \bar{\psi}_2 + \frac{\pi}{2} W''(A) \psi_2 \psi_1. \quad (\text{A41})$$

When $W' = 0$, the traceless condition of Eq. (A30) is clearly satisfied (note that $F = -W'^*$ under the equation of motion).

A.3. $U(1)$ symmetry and the $U(1)$ current

We take the following $U(1)$ transformation ($\gamma \in \mathbb{R}$),

$$\delta \begin{pmatrix} \psi_1 \\ \bar{\psi}_2 \end{pmatrix} (x) = i\gamma \begin{pmatrix} \psi_1 \\ \bar{\psi}_2 \end{pmatrix} (x), \quad \delta \begin{pmatrix} \bar{\psi}_1 \\ \psi_2 \end{pmatrix} (x) = -i\gamma \begin{pmatrix} \bar{\psi}_1 \\ \psi_2 \end{pmatrix} (x), \quad (\text{A42})$$

under which the WZ model is invariant; we have assigned the $U(1)$ charge $+1$ to ψ_1 and $\bar{\psi}_2$, and -1 to $\bar{\psi}_1$ and ψ_2 . It turns out that, in the massless free WZ model, the $U(1)$ current associated with this symmetry forms the superconformal multiplet with the supercurrent and the energy–momentum tensor.¹⁹ Localizing the parameter γ as $\gamma(x)$, the associated

¹⁹The $U(1)_R$ symmetry in the case of the superpotential $W = \lambda \Phi^n/n$ would be

$$A(x) \rightarrow \exp(i\gamma/n) A(x), \quad (\text{A43})$$

$$\psi_\alpha(x) \rightarrow \exp[-i\gamma(n-2)/2n] \psi_\alpha(x), \quad (\text{A44})$$

$$\bar{\psi}_{\dot{\alpha}}(x) \rightarrow \exp[i\gamma(n-2)/2n] \bar{\psi}_{\dot{\alpha}}(x), \quad (\text{A45})$$

$$F(x) \rightarrow \exp[-i\gamma(n-1)/n] F(x). \quad (\text{A46})$$

The associated Noether current, however, can be neither holomorphic nor anti-holomorphic even in the free-field limit $\lambda \rightarrow 0$; thus it cannot be a member of the superconformal multiplet.

Noether current can be obtained as

$$\delta S = \frac{1}{2\pi} \int d^2x 2i\gamma(x) [\partial J_z(x) + \bar{\partial} J_{\bar{z}}(x)]. \quad (\text{A47})$$

The explicit form is given by

$$J \equiv J_z = 2\pi\bar{\psi}_2\psi_2, \quad (\text{A48})$$

$$\bar{J} \equiv J_{\bar{z}} = 2\pi\psi_1\bar{\psi}_1. \quad (\text{A49})$$

It can be confirmed that the supercurrent, the energy–momentum tensor, and the $U(1)$ current in the above form are related by the SUSY transformation in a very simple way. This fact provides more support for the above explicit forms of currents.

A.4. Massless free WZ model

We summarize explicit expressions for the above Noether currents in the massless free WZ model, a free $\mathcal{N} = 2$ SCFT, and confirm that they actually fulfill the $\mathcal{N} = 2$ super-Virasoro algebra as expected.

The supercurrent, the energy–momentum tensor, and the $U(1)$ current in the holomorphic sector are

$$S^+(z) = 4\pi\bar{\psi}_2(z)\partial A(z), \quad (\text{A50})$$

$$S^-(z) = -4\pi\psi_2(z)\partial A^*(z), \quad (\text{A51})$$

$$T(z) = -4\pi\partial A^*(z)\partial A(z) - \pi\psi_2(z)\partial\bar{\psi}_2(z) + \pi\partial\psi_2(z)\bar{\psi}_2(z), \quad (\text{A52})$$

$$J(z) = 2\pi\bar{\psi}_2(z)\psi_2(z), \quad (\text{A53})$$

and in the anti-holomorphic sector,

$$\bar{S}^+(\bar{z}) = -4\pi\psi_1(\bar{z})\bar{\partial} A^*(\bar{z}), \quad (\text{A54})$$

$$\bar{S}^-(\bar{z}) = 4\pi\bar{\psi}_1(\bar{z})\bar{\partial} A(\bar{z}), \quad (\text{A55})$$

$$\bar{T}(\bar{z}) = -4\pi\bar{\partial} A^*(\bar{z})\bar{\partial} A(\bar{z}) - \pi\bar{\psi}_1(\bar{z})\bar{\partial}\psi_1(\bar{z}) + \pi\bar{\partial}\bar{\psi}_1(\bar{z})\psi_1(\bar{z}), \quad (\text{A56})$$

$$\bar{J}(\bar{z}) = 2\pi\psi_1(\bar{z})\bar{\psi}_1(\bar{z}). \quad (\text{A57})$$

The OPEs between the component fields are given by

$$A(z, \bar{z})A^*(0, 0) \sim -\frac{1}{4\pi} \ln |z|^2, \quad (\text{A58})$$

$$\psi_1(\bar{z})\bar{\psi}_1(0) \sim \frac{1}{2\pi} \frac{1}{\bar{z}}, \quad (\text{A59})$$

$$\bar{\psi}_2(z)\psi_2(0) \sim \frac{1}{2\pi} \frac{1}{z}, \quad (\text{A60})$$

$$(\text{otherwise}) \sim 0, \quad (\text{A61})$$

where “ \sim ” implies “ $=$ ” up to non-singular terms. Using these, we find that the above Noether currents in the holomorphic part satisfy the OPEs of the $\mathcal{N} = 2$ super-Virasoro algebra,

$$T(z)T(0) \sim \frac{c}{2z^4} + \frac{2}{z^2}T(0) + \frac{1}{z}\partial T(0), \quad (\text{A62})$$

$$T(z)S^\pm(0) \sim \frac{3}{2z^2}S^\pm(0) + \frac{1}{z}\partial S^\pm(0), \quad (\text{A63})$$

$$T(z)J(0) \sim \frac{1}{z^2}J(0) + \frac{1}{z}\partial J(0), \quad (\text{A64})$$

$$S^\pm(z)S^\pm(0) \sim 0, \quad (\text{A65})$$

$$S^+(z)S^-(0) \sim \frac{2c}{3z^3} + \frac{2}{z^2}J(0) + \frac{2}{z}T(0) + \frac{1}{z}\partial J(0), \quad (\text{A66})$$

$$J(z)S^\pm(0) \sim \pm \frac{1}{z}S^\pm(0), \quad (\text{A67})$$

$$J(z)J(0) \sim \frac{c}{3z^2}, \quad (\text{A68})$$

where the central charge is $c = 3$ corresponding to a free $\mathcal{N} = 2$ SCFT.

B. A fast algorithm for the Jacobian computation

We can accelerate the computation of $\text{sign det} \frac{\partial(N, N^*)}{\partial(A, A^*)}$ by effectively halving the size of the matrix,

$$\frac{\partial(N, N^*)}{\partial(A, A^*)} = \begin{pmatrix} 2ip_z & W''(A)^{**} \\ W''(A)^* & 2ip_{\bar{z}} \end{pmatrix}, \quad (\text{B1})$$

whose p, q element is

$$\begin{aligned} \left[\frac{\partial(N, N^*)}{\partial(A, A^*)} \right]_{p,q} &= \begin{pmatrix} 2ip_z \delta_{p,q} & \frac{1}{L_0 L_1} W''(A)(q-p)^* \\ \frac{1}{L_0 L_1} W''(A)(p-q) & 2ip_{\bar{z}} \delta_{p,q} \end{pmatrix} \\ &= \begin{pmatrix} 2ip_z \delta_{p,q} & \frac{1}{L_0 L_1} W''(A)(p-q)^\dagger \\ \frac{1}{L_0 L_1} W''(A)(p-q) & 2ip_{\bar{z}} \delta_{p,q} \end{pmatrix}. \end{aligned} \quad (\text{B2})$$

Note that Eq. (B2) is a $[2(L_0 + 1)(L_1 + 1)] \times [2(L_0 + 1)(L_1 + 1)]$ matrix when the momentum takes the values

$$p_\mu = \frac{2\pi}{L_\mu} n_\mu, \quad n_\mu = 0, \pm 1, \dots, \pm \frac{L_\mu}{2}, \quad (\text{B3})$$

where we have assumed that both integers L_0 and L_1 are even,

We write the matrix in Eq. (B2) as

$$\frac{\partial(N, N^*)}{\partial(A, A^*)} \equiv \begin{pmatrix} iP & W^\dagger \\ W & iP^\dagger \end{pmatrix}. \quad (\text{B4})$$

It should be noted that the diagonal matrix P , whose p, q element is $2p_z \delta_{p,q}$, does not have an inverse because it has zero at $p = 0$; what we want to do is to remove this zero.

Considering the case that P and W are 3×3 matrices for simplicity, we can confirm that the determinant of the matrix in Eq. (B4) can be deformed as

$$\det \begin{pmatrix} \lambda_1 & & & & \\ & 0 & & & \\ & & \lambda_2 & & \\ W_{11} & W_{12} & W_{13} & \lambda_3 & \\ W_{21} & W_{22} & W_{23} & & 0 \\ W_{31} & W_{32} & W_{33} & & \lambda_4 \end{pmatrix} = -|W_{22}|^2 \det \begin{pmatrix} \lambda_1 & & \widetilde{W}_{11}^* & \widetilde{W}_{31}^* \\ & \lambda_2 & \widetilde{W}_{13}^* & \widetilde{W}_{33}^* \\ \widetilde{W}_{11} & \widetilde{W}_{13} & \lambda_3 & \\ \widetilde{W}_{31} & \widetilde{W}_{33} & & \lambda_4 \end{pmatrix}, \quad (\text{B5})$$

where

$$\widetilde{W}_{ij} \equiv \frac{1}{W_{22}} \det \begin{pmatrix} W_{ij} & W_{i2} \\ W_{2j} & W_{22} \end{pmatrix}. \quad (\text{B6})$$

In an analogous way, we can write, for the general case,

$$\det \begin{pmatrix} iP & W^\dagger \\ W & iP^\dagger \end{pmatrix} = -|W_{0,0}|^2 \det' \begin{pmatrix} iP & \widetilde{W}^\dagger \\ \widetilde{W} & iP^\dagger \end{pmatrix}, \quad (\text{B7})$$

where $W_{0,0}$ is the component at $(p, q) = (0, 0)$, \det' is the determinant in the subspace in which the components with $p = 0$ or $q = 0$ are omitted, and

$$\widetilde{W}_{p,q} = \frac{1}{W_{0,0}} \det \begin{pmatrix} W_{p,q} & W_{p,0} \\ W_{0,q} & W_{0,0} \end{pmatrix}. \quad (\text{B8})$$

Note that this is simply the determinant of a 2×2 matrix.

Since the right-hand side of Eq. (B7) refers to the subspace in which P has an inverse, the Jacobian can be expressed as

$$\det \begin{pmatrix} iP & W^\dagger \\ W & iP^\dagger \end{pmatrix} = -|W_{0,0}|^2 \det' \begin{pmatrix} iP & 0 \\ \widetilde{W} & I \end{pmatrix} \det' \begin{pmatrix} I & (-i)P^{-1}\widetilde{W}^\dagger \\ 0 & iP^\dagger - \widetilde{W}(-i)P^{-1}\widetilde{W}^\dagger \end{pmatrix} \quad (\text{B9})$$

$$= -|W_{0,0}|^2 \det' \left(-PP^\dagger - P\widetilde{W}P^{-1}\widetilde{W}^\dagger \right). \quad (\text{B10})$$

Here, the inverse of P is given by

$$(P^{-1})_{p,q} = \frac{1}{2p_z} \delta_{p,q} = \frac{p_z}{2|p_z|^2} \delta_{p,q}. \quad (\text{B11})$$

Thus, substituting the matrix elements in Eq. (B2), we have

$$\begin{aligned} \det \begin{pmatrix} iP & W^\dagger \\ W & iP^\dagger \end{pmatrix} &= -\det'(-1) \left| \frac{1}{L_0 L_1} W''(A)(0) \right|^2 \\ &\times \det' \left[4|p_z|^2 \delta_{p,q} + \left(\frac{1}{L_0 L_1} \right)^2 \sum_{l \neq 0} \frac{p_z}{l_z} \widetilde{W}''(A)(p-l) \widetilde{W}''(A)(l-q)^\dagger \right], \end{aligned} \quad (\text{B12})$$

where for $p \neq 0$,

$$\begin{aligned} \widetilde{W}''(A)(p-l) &\equiv \frac{1}{W''(A)(0)} \det \begin{pmatrix} W''(A)(p-l) & W''(A)(p-0) \\ W''(A)(0-l) & W''(A)(0-0) \end{pmatrix} \\ &= \frac{1}{W''(A)(0)} [W''(A)(p-l)W''(A)(0) - W''(A)(p)W''(A)(-l)]. \end{aligned} \quad (\text{B13})$$

Here, the factor $\det'(-1)$ is

$$\det'(-1) = (-1)^{(L_0+1)(L_1+1)-1} = +1, \quad (\text{B14})$$

for L_0 and L_1 are even.

Thus, finally, the sign of the Jacobian is given by the sign of the determinant of a matrix with smaller dimensions $[(L_0 + 1)(L_1 + 1) - 1] \times [(L_0 + 1)(L_1 + 1) - 1]$, as

$$\begin{aligned} & \text{sign det} \begin{pmatrix} iP & W^\dagger \\ W & iP^\dagger \end{pmatrix} \\ &= -\det'(-1) \text{sign det}' \left[4|p_z|^2 \delta_{p,q} + \left(\frac{1}{L_0 L_1} \right)^2 \sum_{l \neq 0} \frac{p_z}{l_z} \widetilde{W}''(A)(p-l) \widetilde{W}''(A)(q-l)^* \right]. \end{aligned} \quad (\text{B15})$$

Since the computational cost required for the matrix determinant is $O(N^3)$ for a matrix of size N , this representation reduces the cost by $\sim 1/8$.

It turns out that the above sign is mainly negative for most of configurations of $A(p)$. Since the overall sign of $\text{sign det} \frac{\partial(N, N^*)}{\partial(A, A^*)}$ is irrelevant in the expectation value of Eq. (2.24), we regard Eq. (B15) as²⁰

$$-\text{sign det} \frac{\partial(N, N^*)}{\partial(A, A^*)}. \quad (\text{B16})$$

References

- [1] A. B. Zamolodchikov, Sov. J. Nucl. Phys. **44** (1986) 529 [Yad. Fiz. **44** (1986) 821].
- [2] J. Wess and B. Zumino, Nucl. Phys. B **70** (1974) 39. doi:10.1016/0550-3213(74)90355-1
- [3] P. Di Vecchia, J. L. Petersen and H. B. Zheng, Phys. Lett. **162B** (1985) 327. doi:10.1016/0370-2693(85)90932-3
- [4] P. Di Vecchia, J. L. Petersen and M. Yu, Phys. Lett. B **172** (1986) 211. doi:10.1016/0370-2693(86)90837-3
- [5] P. Di Vecchia, J. L. Petersen, M. Yu and H. B. Zheng, Phys. Lett. B **174** (1986) 280. doi:10.1016/0370-2693(86)91099-3
- [6] W. Boucher, D. Friedan and A. Kent, Phys. Lett. B **172** (1986) 316. doi:10.1016/0370-2693(86)90260-1
- [7] D. Gepner, Nucl. Phys. B **287** (1987) 111. doi:10.1016/0550-3213(87)90098-8
- [8] A. Cappelli, C. Itzykson and J. B. Zuber, Nucl. Phys. B **280** (1987) 445. doi:10.1016/0550-3213(87)90155-6
- [9] A. Cappelli, Phys. Lett. B **185** (1987) 82. doi:10.1016/0370-2693(87)91532-2
- [10] D. Gepner and Z. a. Qiu, Nucl. Phys. B **285** (1987) 423. doi:10.1016/0550-3213(87)90348-8
- [11] D. Gepner, Nucl. Phys. B **296** (1988) 757. doi:10.1016/0550-3213(88)90397-5
- [12] A. Cappelli, C. Itzykson and J. B. Zuber, Commun. Math. Phys. **113** (1987) 1. doi:10.1007/BF01221394
- [13] A. Kato, Mod. Phys. Lett. A **2** (1987) 585. doi:10.1142/S0217732387000732
- [14] D. Gepner, Phys. Lett. B **199** (1987) 380. doi:10.1016/0370-2693(87)90938-5
- [15] D. A. Kastor, E. J. Martinec and S. H. Shenker, Nucl. Phys. B **316** (1989) 590. doi:10.1016/0550-3213(89)90060-6
- [16] C. Vafa and N. P. Warner, Phys. Lett. B **218** (1989) 51. doi:10.1016/0370-2693(89)90473-5
- [17] E. J. Martinec, Phys. Lett. B **217** (1989) 431. doi:10.1016/0370-2693(89)90074-9
- [18] W. Lerche, C. Vafa and N. P. Warner, Nucl. Phys. B **324** (1989) 427. doi:10.1016/0550-3213(89)90474-4
- [19] P. S. Howe and P. C. West, Phys. Lett. B **223** (1989) 377. doi:10.1016/0370-2693(89)91619-5
- [20] S. Cecotti, L. Girardello and A. Pasquinucci, Nucl. Phys. B **328** (1989) 701. doi:10.1016/0550-3213(89)90226-5
- [21] P. S. Howe and P. C. West, Phys. Lett. B **227** (1989) 397. doi:10.1016/0370-2693(89)90950-7
- [22] S. Cecotti, L. Girardello and A. Pasquinucci, Int. J. Mod. Phys. A **6** (1991) 2427. doi:10.1142/S0217751X91001192

²⁰ Or we may simply say that the partition function (2.19) is defined with another negative sign.

- [23] S. Cecotti, *Int. J. Mod. Phys. A* **6** (1991) 1749. doi:10.1142/S0217751X91000939
- [24] E. Witten, *Int. J. Mod. Phys. A* **9** (1994) 4783 doi:10.1142/S0217751X9400193X [hep-th/9304026].
- [25] H. Kawai and Y. Kikukawa, *Phys. Rev. D* **83** (2011) 074502 doi:10.1103/PhysRevD.83.074502 [arXiv:1005.4671 [hep-lat]].
- [26] Y. Kikukawa and Y. Nakayama, *Phys. Rev. D* **66** (2002) 094508 doi:10.1103/PhysRevD.66.094508 [hep-lat/0207013].
- [27] H. Nicolai, *Phys. Lett.* **89B** (1980) 341. doi:10.1016/0370-2693(80)90138-0
- [28] H. Nicolai, *Nucl. Phys. B* **176** (1980) 419. doi:10.1016/0550-3213(80)90460-5
- [29] G. Parisi and N. Surlas, *Nucl. Phys. B* **206** (1982) 321. doi:10.1016/0550-3213(82)90538-7
- [30] S. Cecotti and L. Girardello, *Annals Phys.* **145** (1983) 81. doi:10.1016/0003-4916(83)90172-0
- [31] N. Sakai and M. Sakamoto, *Nucl. Phys. B* **229**, 173 (1983). doi:10.1016/0550-3213(83)90359-0
- [32] J. Giedt and E. Poppitz, *JHEP* **0409**, 029 (2004) doi:10.1088/1126-6708/2004/09/029 [hep-th/0407135].
- [33] D. Kadoh and H. Suzuki, *Phys. Lett. B* **696**, 163 (2011) doi:10.1016/j.physletb.2010.12.012 [arXiv:1011.0788 [hep-lat]].
- [34] D. Kadoh, *PoS LATTICE 2015* (2016) 017 [arXiv:1607.01170 [hep-lat]].
- [35] M. Beccaria, G. Curci and E. D'Ambrosio, *Phys. Rev. D* **58**, 065009 (1998) doi:10.1103/PhysRevD.58.065009 [hep-lat/9804010].
- [36] S. Catterall and S. Karamov, *Phys. Rev. D* **65**, 094501 (2002) doi:10.1103/PhysRevD.65.094501 [hep-lat/0108024].
- [37] J. Giedt, *Nucl. Phys. B* **726**, 210 (2005) doi:10.1016/j.nuclphysb.2005.08.004 [hep-lat/0507016].
- [38] G. Bergner, T. Kaestner, S. Uhlmann and A. Wipf, *Annals Phys.* **323**, 946 (2008) doi:10.1016/j.aop.2007.06.010 [arXiv:0705.2212 [hep-lat]].
- [39] T. Kastner, G. Bergner, S. Uhlmann, A. Wipf and C. Wozar, *Phys. Rev. D* **78**, 095001 (2008) doi:10.1103/PhysRevD.78.095001 [arXiv:0807.1905 [hep-lat]].
- [40] S. Nicolis, arXiv:1712.07045 [hep-th].
- [41] S. Kamata and H. Suzuki, *Nucl. Phys. B* **854** (2012) 552 doi:10.1016/j.nuclphysb.2011.09.007 [arXiv:1107.1367 [hep-lat]].
- [42] D. Kadoh and H. Suzuki, *Phys. Lett. B* **684** (2010) 167 doi:10.1016/j.physletb.2010.01.022 [arXiv:0909.3686 [hep-th]].
- [43] J. Bartels and J. B. Bronzan, *Phys. Rev. D* **28** (1983) 818. doi:10.1103/PhysRevD.28.818
- [44] S. D. Drell, M. Weinstein and S. Yankielowicz, *Phys. Rev. D* **14** (1976) 487. doi:10.1103/PhysRevD.14.487
- [45] S. D. Drell, M. Weinstein and S. Yankielowicz, *Phys. Rev. D* **14** (1976) 1627. doi:10.1103/PhysRevD.14.1627
- [46] G. Bergner, *JHEP* **1001**, 024 (2010) doi:10.1007/JHEP01(2010)024 [arXiv:0909.4791 [hep-lat]].
- [47] P. H. Dondi and H. Nicolai, *Nuovo Cim. A* **41** (1977) 1. doi:10.1007/BF02730448
- [48] L. H. Karsten and J. Smit, *Phys. Lett.* **85B** (1979) 100. doi:10.1016/0370-2693(79)90786-X
- [49] M. Kato, M. Sakamoto and H. So, *JHEP* **0805** (2008) 057 doi:10.1088/1126-6708/2008/05/057 [arXiv:0803.3121 [hep-lat]].
- [50] A. B. Zamolodchikov, *JETP Lett.* **43** (1986) 730 [*Pisma Zh. Eksp. Teor. Fiz.* **43** (1986) 565].
- [51] A. Cappelli and J. I. Latorre, *Nucl. Phys. B* **340** (1990) 659. doi:10.1016/0550-3213(90)90463-N
- [52] S. Cecotti, *Nucl. Phys. B* **355** (1991) 755. doi:10.1016/0550-3213(91)90493-H
- [53] B. R. Greene, C. Vafa and N. P. Warner, *Nucl. Phys. B* **324** (1989) 371. doi:10.1016/0550-3213(89)90471-9
- [54] E. Witten, *Nucl. Phys. B* **403** (1993) 159 [*AMS/IP Stud. Adv. Math.* **1** (1996) 143] doi:10.1016/0550-3213(93)90033-L [hep-th/9301042].
- [55] M. Lüscher, *Commun. Math. Phys.* **293**, 899 (2010) doi:10.1007/s00220-009-0953-7 [arXiv:0907.5491 [hep-lat]].
- [56] E. Witten, *Nucl. Phys. B* **202** (1982) 253. doi:10.1016/0550-3213(82)90071-2
- [57] S. Cecotti and L. Girardello, *Phys. Lett.* **110B** (1982) 39. doi:10.1016/0370-2693(82)90947-9
- [58] <http://eigen.tuxfamily.org/>
- [59] <http://julialang.org/>
- [60] J. Bezanson, S. Karpinski, V. B. Shah and A. Edelman, arXiv:1209.5145 [cs.PL].
- [61] J. Bezanson, A. Edelman, S. Karpinski and V. B. Shah, arXiv:1411.1607 [cs.MS].
- [62] J. Polchinski, "String theory. Vol. 1: An introduction to the bosonic string," Cambridge University Press, 1998, 402 p.
- [63] J. Polchinski, "String theory. Vol. 2: Superstring theory and beyond," Cambridge University Press, 1998, 531 p.